Supporting Information

# Oxytetracycline-derived carbon dots for the fluorescence switch of trace ferric ion sensing

Tao Chen[1,2,3,4+], Yan-Tong Xu[2,3,4+], Qing Guo[1,2,3,4], Xiaoli Chen[2,3,4], Qiucheng Su[2,3,4] and Yan Cao*[1,2,3,4]

1. College of Chemistry and Chemical Engineering, Anhui University, Hefei 230601, China.
2. Guangzhou Institute of Energy Conversion, Chinese Academy of Sciences, Guangzhou 510640, China.
3. Guangdong Provincial Key Laboratory of New and Renewable Energy Research and Development, Guangzhou 510640, China.
4. CAS Key Laboratory of Renewable Energy, Guangzhou 510640, China.

[+] These authors contributed equally to this work.

* Corresponding author: Prof. Yan Cao (E-mail: caoyan@ms.giec.ac.cn)

**Instrumentation methods**

The size and morphology of the as-prepared OCDs were characterized using a transmission electron microscope (TEM, JEM-2100F microscope). The OCDs were ultrasonically dispersed in ethanol and TEM samples were prepared by adding two drops of OCDs ethanol solution on an ultrathin carbon film and then dried at room temperature overnight. Raman spectroscopy (LabRAM HR800) was conducted under a 532 nm excitation laser. The functional groups and chemical components were tested using a FT-IR Prestige-21 with a KBr disk in the range of 4000 to 500 $cm^{-1}$ and an X-ray photoelectron spectrometer (XPS, ESCALAB 250Xi X-ray photoelectron spectrometer), respectively. The sample preparation for the FT-IR measurement was conducted by firstly mixing the as-prepared OCDs and KBr, then uniformly grinding and pressing them to make sample tablets prior to the FT-IR testing. The Fluorescence spectrum was performed on a Hitachi F-2500 typed and Perkin Elmer LS-55 typed fluorescence spectrophotometers using quartz cuvettes. The slit bands of both the excitation and emission were 5 nm. Fluorescence cell images were collected by the home-built multifunctional microscope equipped with bright-field and fluorescent modules.

**Quantum yield measurement of OCDs**

The quantum yield (QY) of the synthesized OCDs s was calculated by using quinine sulfate in 0.1 M $H_2SO_4$ ($QY_2$ is 0.54) as a standard reference and was calculated using the following equation(Eq.S1):

$$QY_1=QY_2\frac{S_1}{S_2}\frac{A_2}{A_1}\frac{n_1^2}{n_2^2} \qquad \text{(Eq.S1)}$$

where, “S” is the integrated area of the fluorescence emission spectrum., “A” is the absorbance, and “n” is the refractive index of the solvent. The representation of subscript "1" is the parameter of OCDs, and the representation of subscript "2" is the parameter of quinoline sulfate in reference solution.

**Product yield measurement of OCDs**

The product yield (PY) of the synthesized OCDs was determined according to Eq.S2:

$$PY=(m_{OCDs}/m_p)\times 100\% \qquad \text{(Eq.S2)}$$

where $m_{OCDs}$ and $m_p$ refer to the mass of as-prepared OCDs powder and precursor respectively.

**Mechanism on masking effect of cysteine**

The mercury is a thiophilic element and thus the mercaptide is formed after adding cysteine to the Hg(II)-containing solution, resulting in a dramatic drop of Hg(II) concentration. Moreover, not only the formation of Hg-mercaptide can avoid the interaction between Hg(II) with OCDs, but also it is non-fluorescent. Consequently, it displays the masking effect on Hg(II) ions.

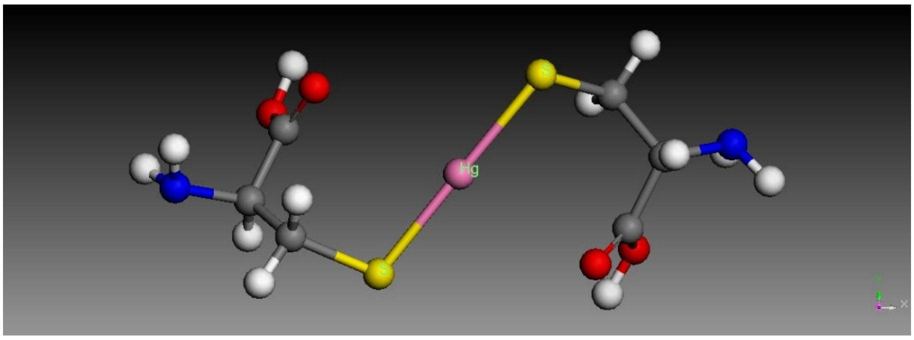


Structure of Hg(II)- cysteine complex

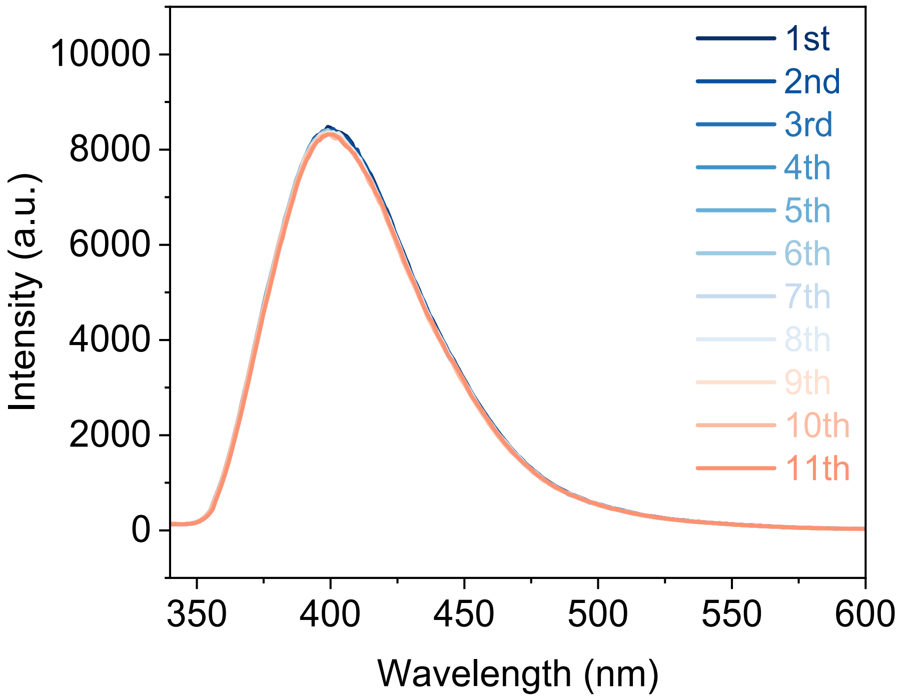


**Fig. S1** Fluorescence emission spectra of OCDs (11 repetitions of the test).

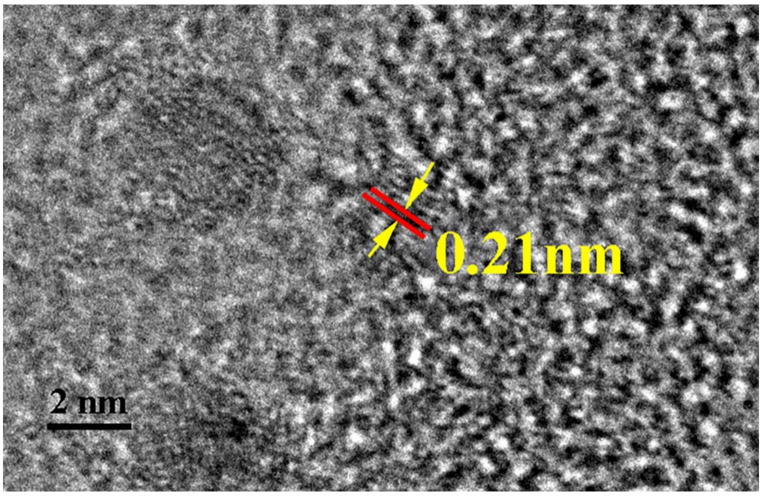


**Fig. S2** HRTEM images of synthesized OCDs.

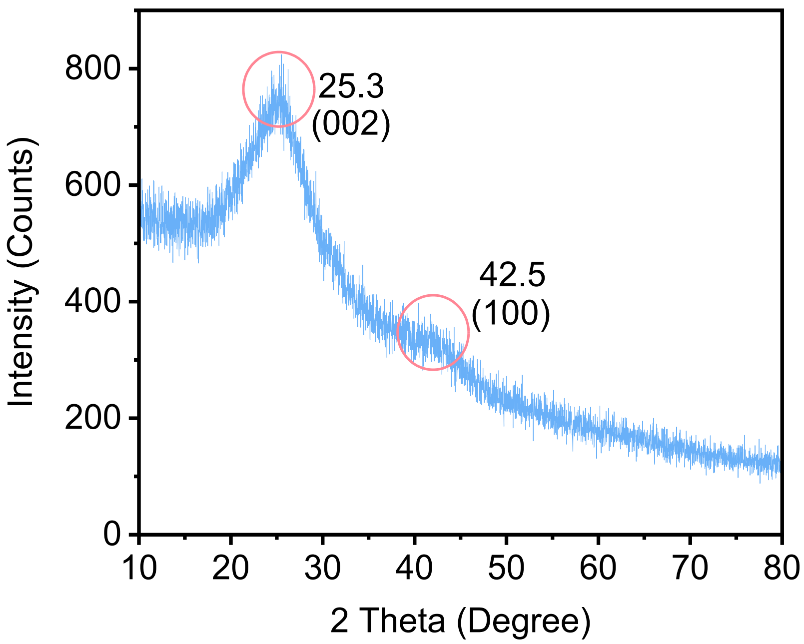


**Fig. S3** XRD patterns of synthesized OCDs.

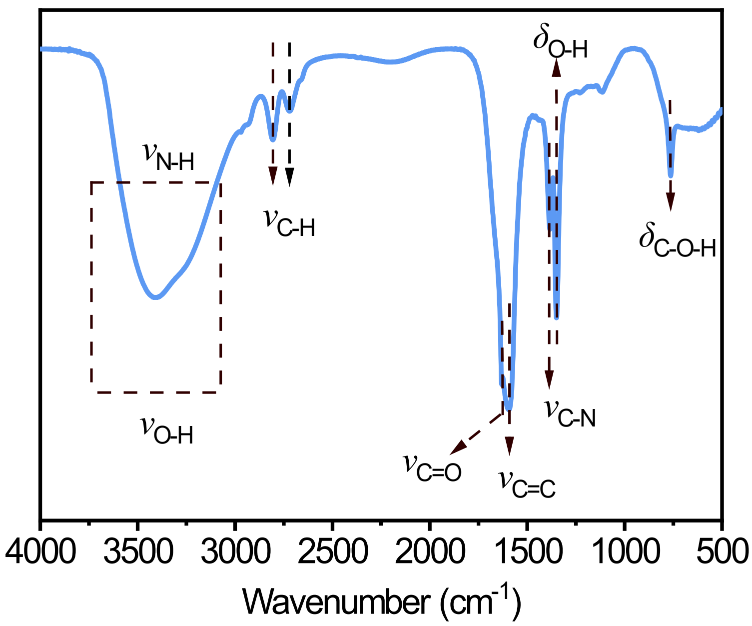


**Fig. S4** FT-IR spectrum of synthesized OCDs.

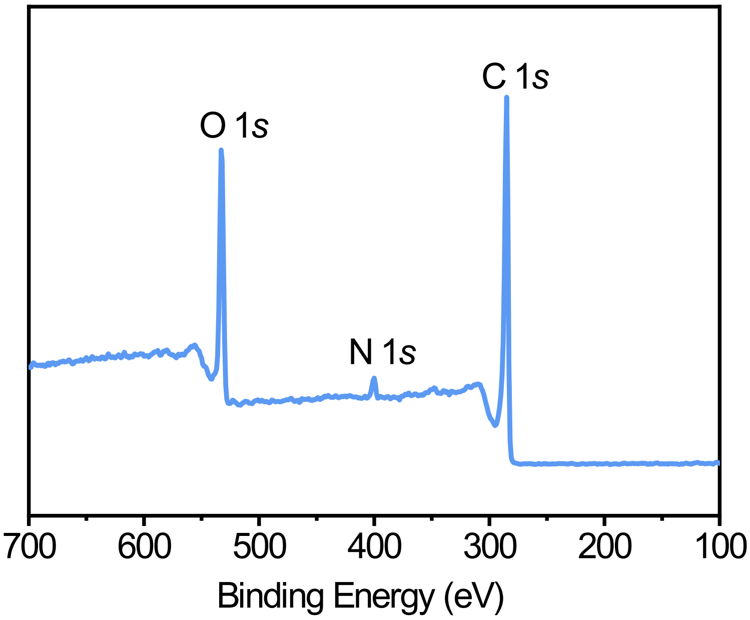


**Fig. S5** Survey of XPS spectra of synthesized OCDs.

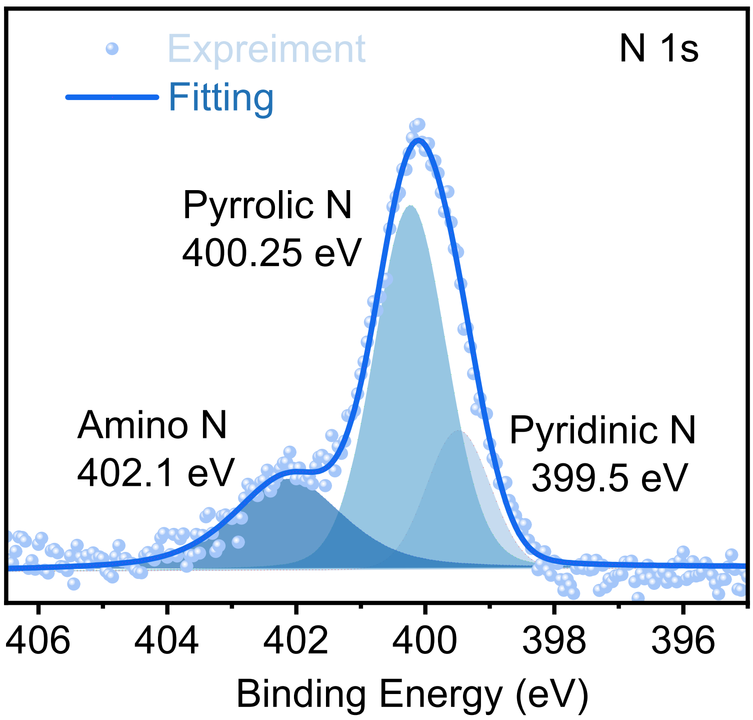


**Fig. S6** High-resolution N1s profile of XPS spectra of synthesized OCDs.

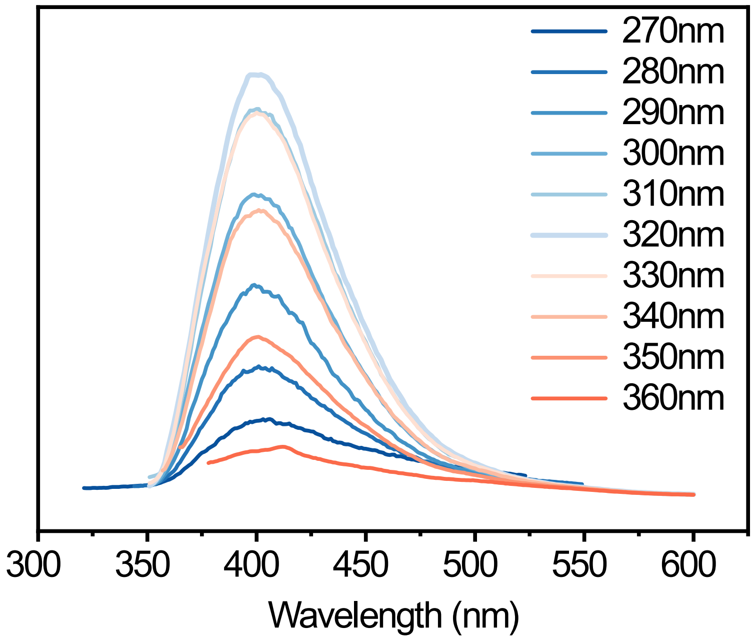


**Fig. S7** Fluorescence emission spectra of OCDs at different excitation wavelengths.

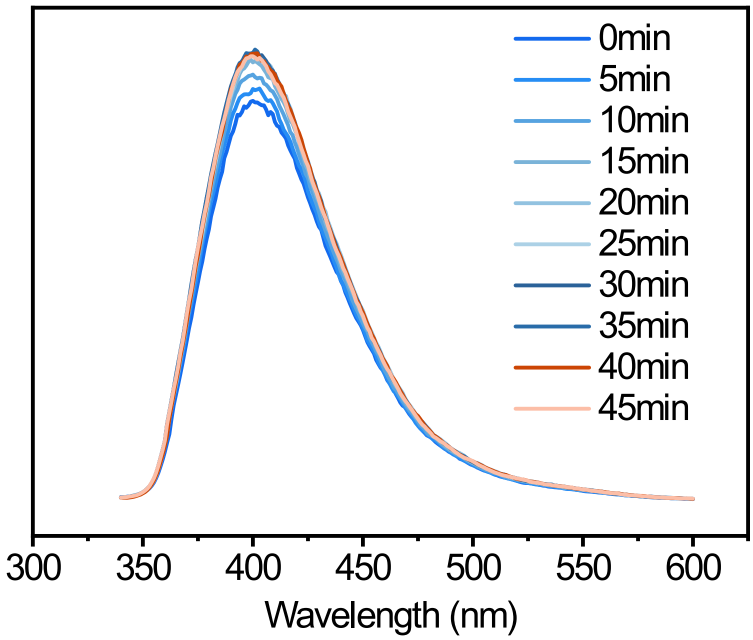


**Fig. S8** Fluorescence emission spectra of OCDs at different time.

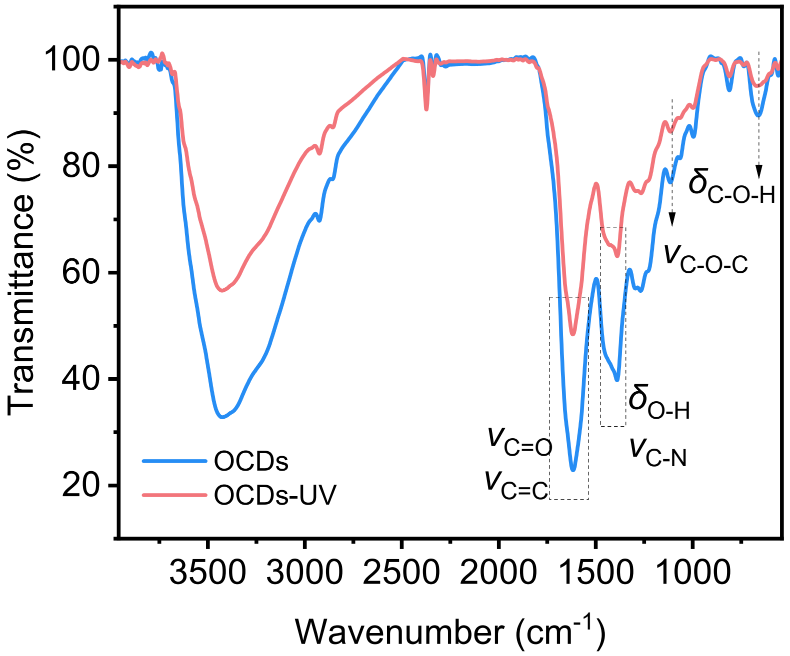


**Fig. S9** FT-IR spectrum of OCDs powder before and after 1h ultraviolet irradiation.

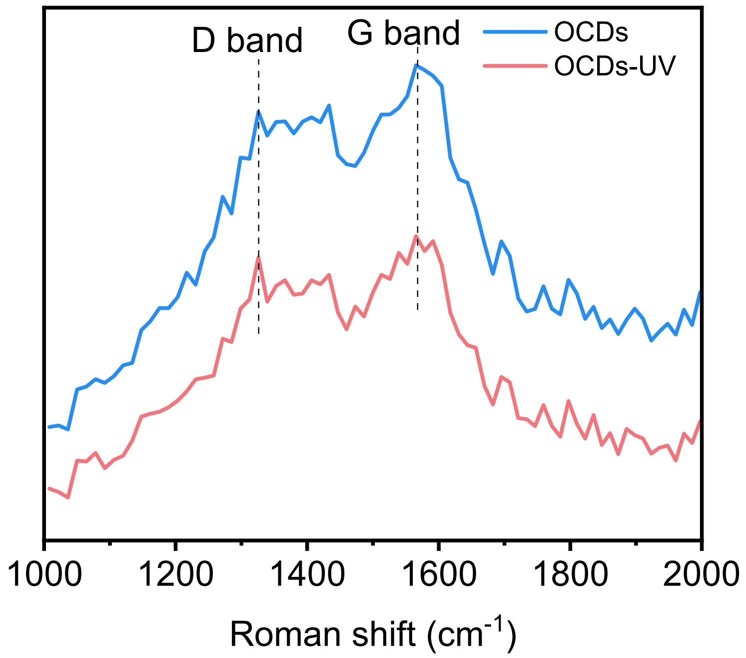


**Fig. S10** Raman spectrum of OCDs powder before and after 1h ultraviolet irradiation.

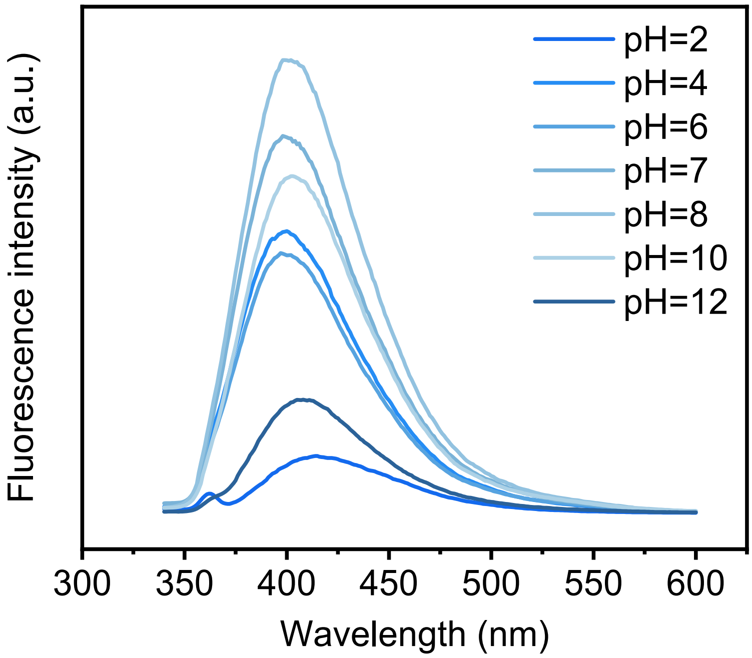


**Fig. S11** Fluorescence emission spectra of OCDs at different pH conditions.

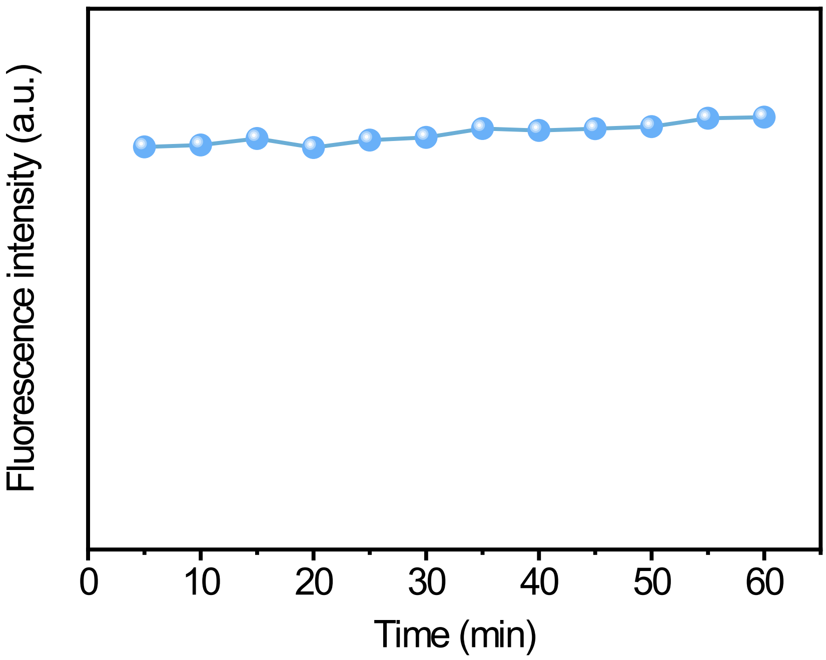


**Fig. S12** Fluorescence emission intensities of OCDs-Fe(III) change upon the increase of time.

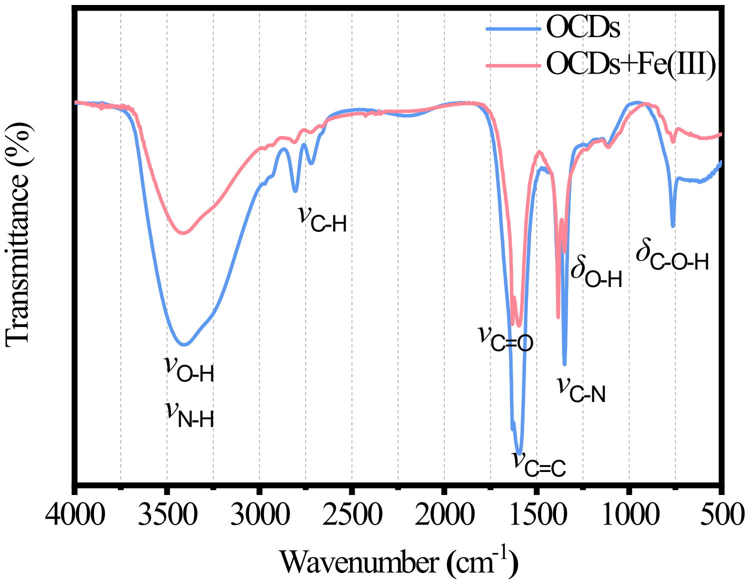


**Fig. S13** FT-IR spectrum of OCDs and Fe(III)-OCDs.

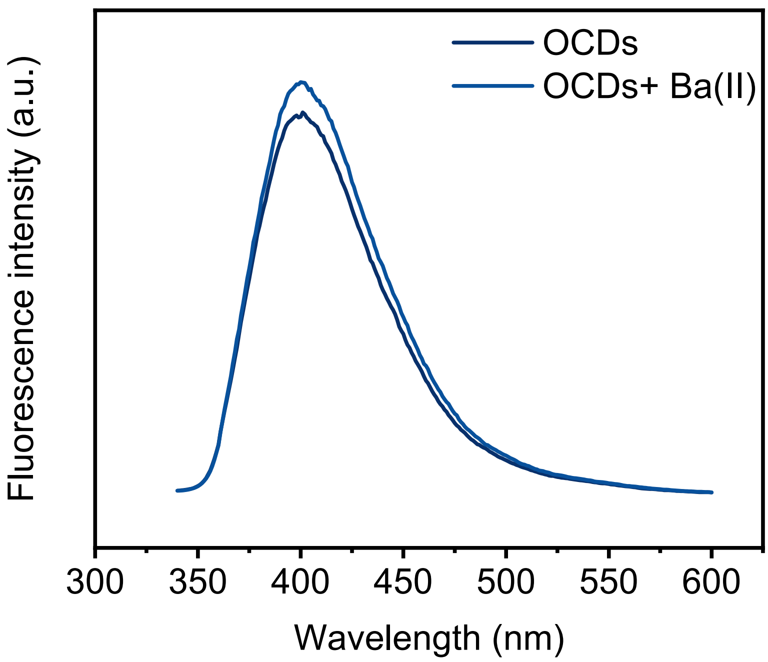


**Fig. S14** Fluorescence spectra of OCDs with and without Ba(II).

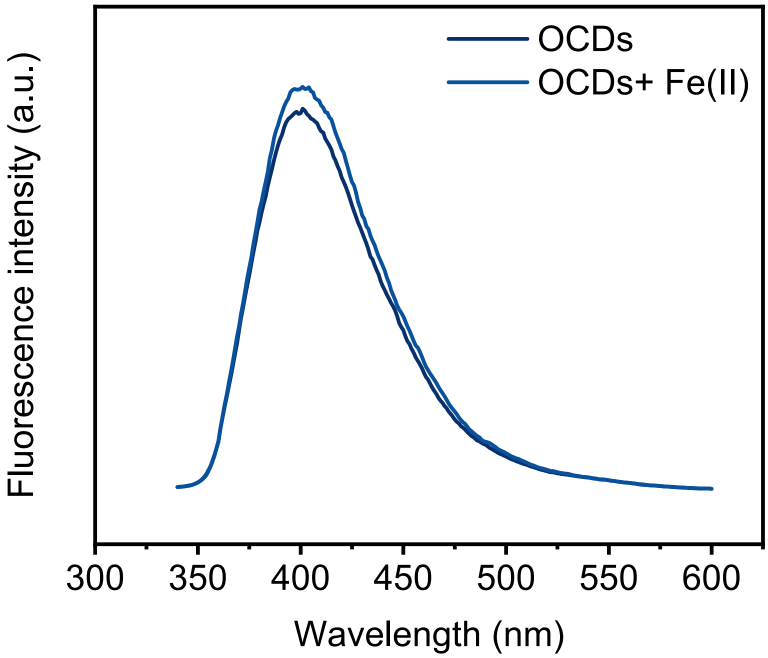


**Fig. S15** Fluorescence spectra of OCDs with and without Fe(II).

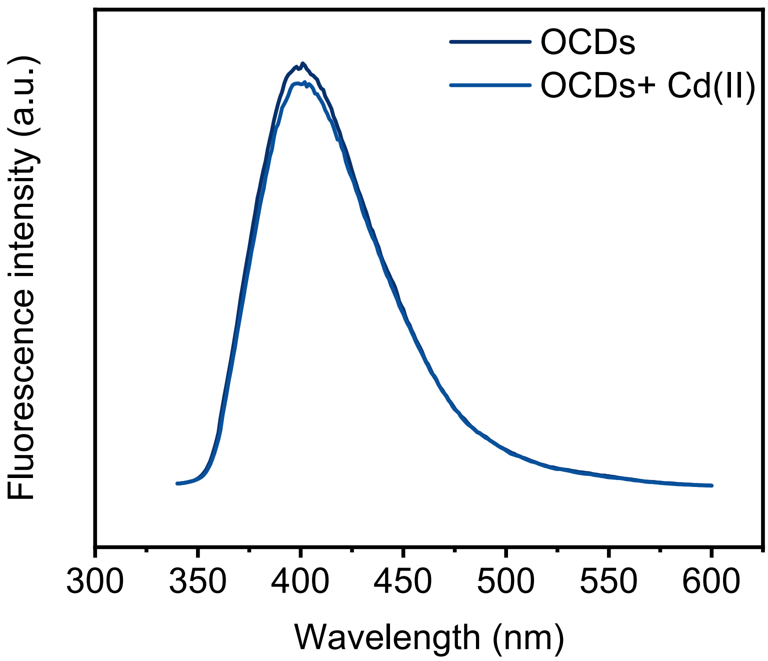


**Fig. S16** Fluorescence spectra of OCDs with and without Cd(II).

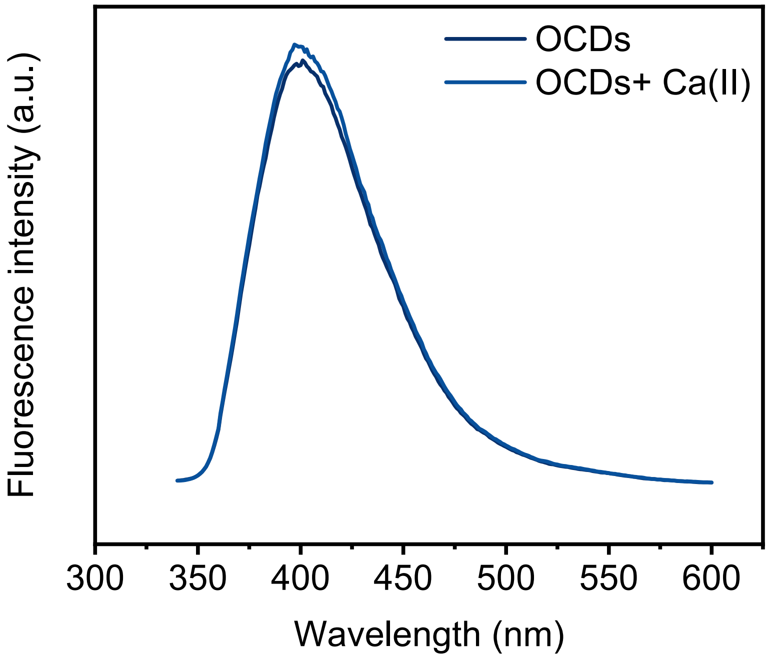


**Fig. S17** Fluorescence spectra of OCDs with and without Ca(II).

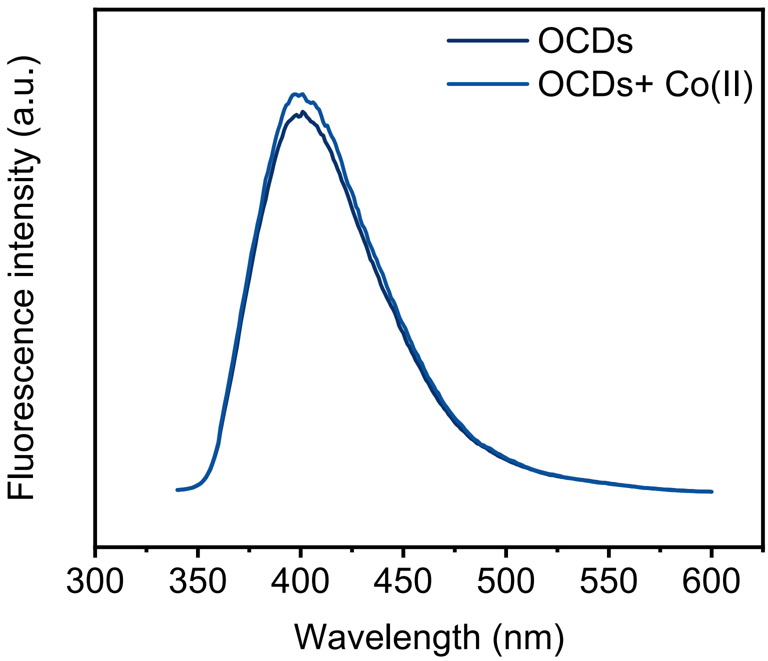


**Fig. S18** Fluorescence spectra of OCDs with and without Co(II).

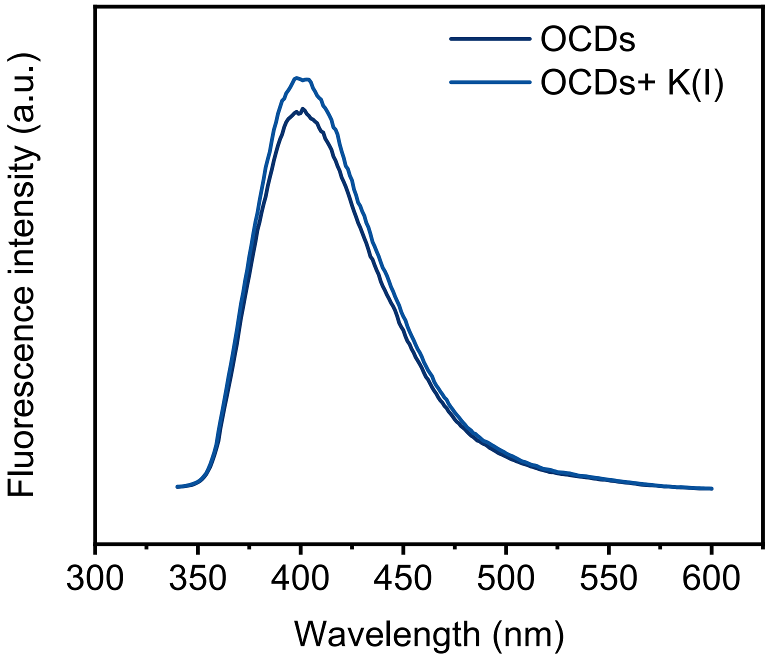


**Fig. S19** Fluorescence spectra of OCDs with and without K(I).

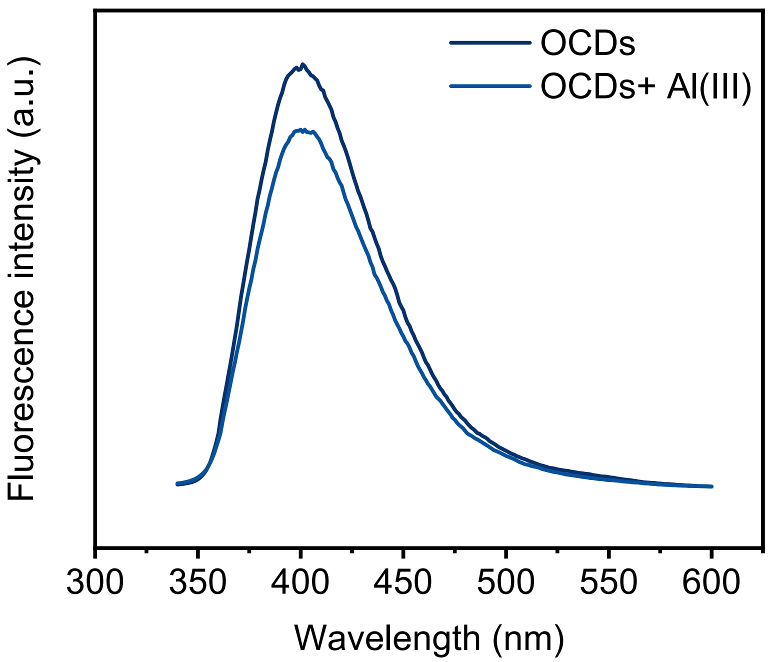


**Fig. S20** Fluorescence spectra of OCDs with and without Al(III).

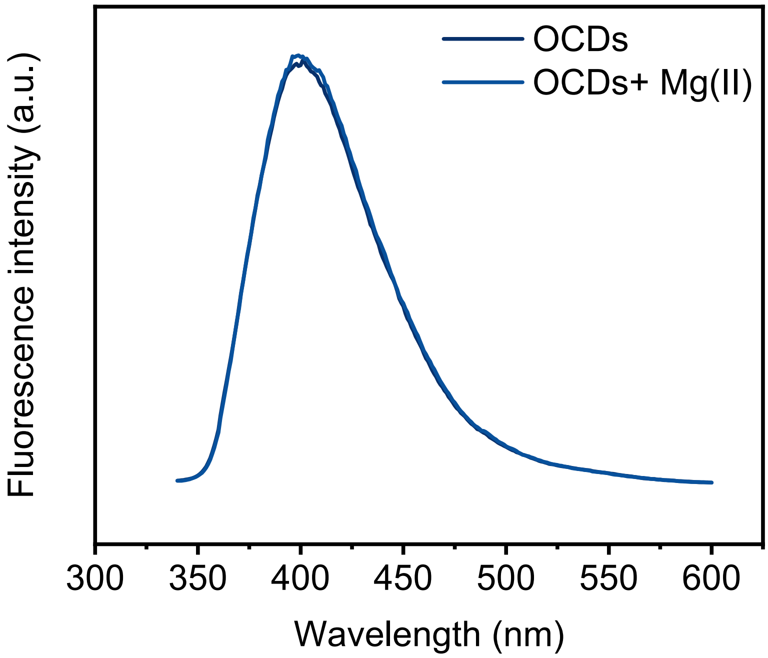


**Fig. S21** Fluorescence spectra of OCDs with and without Mg(II).

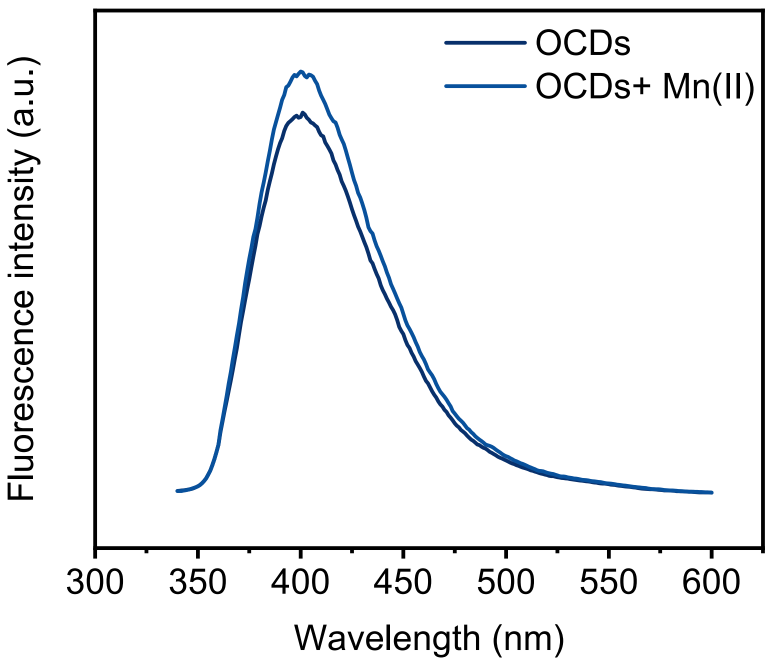


**Fig. S22** Fluorescence spectra of OCDs with and without Mn(II).

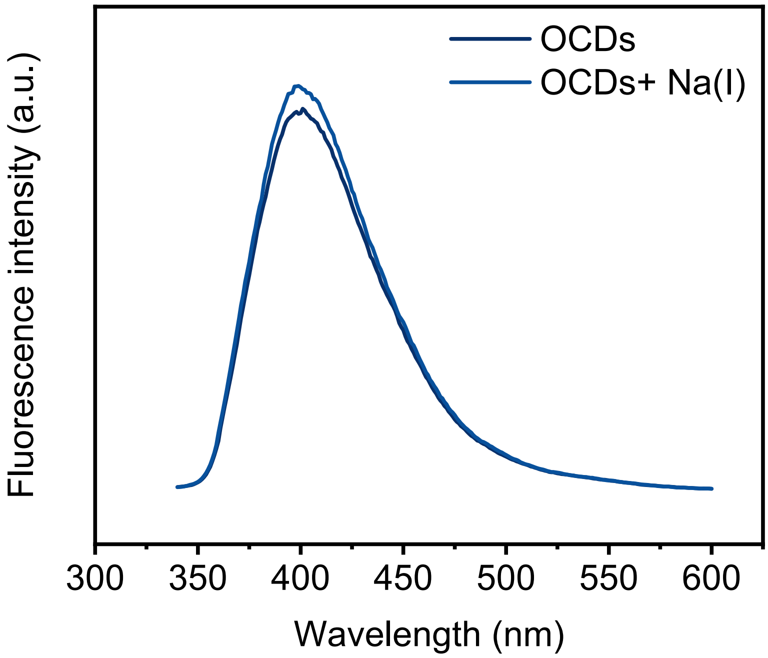


**Fig. S23** Fluorescence spectra of OCDs with and without Na(I).

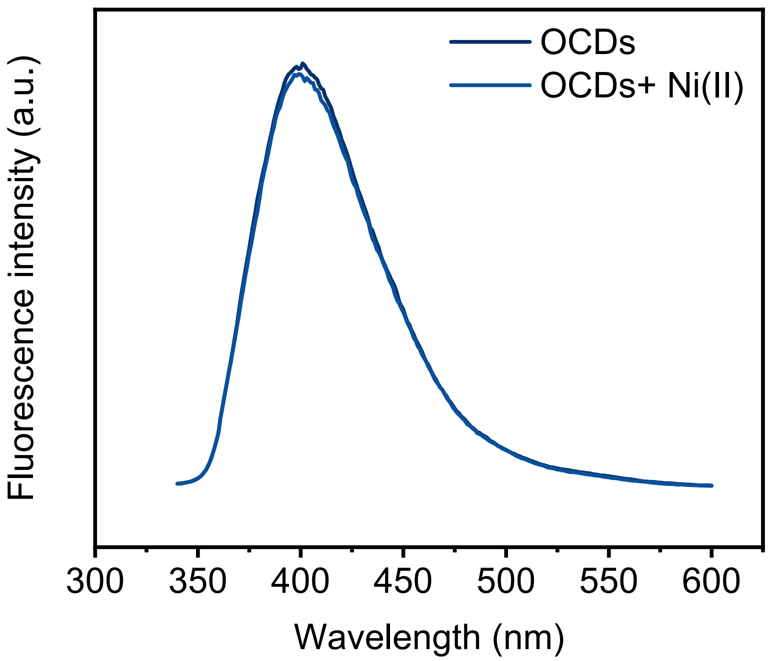


**Fig. S24** Fluorescence spectra of OCDs with and without Ni(II).

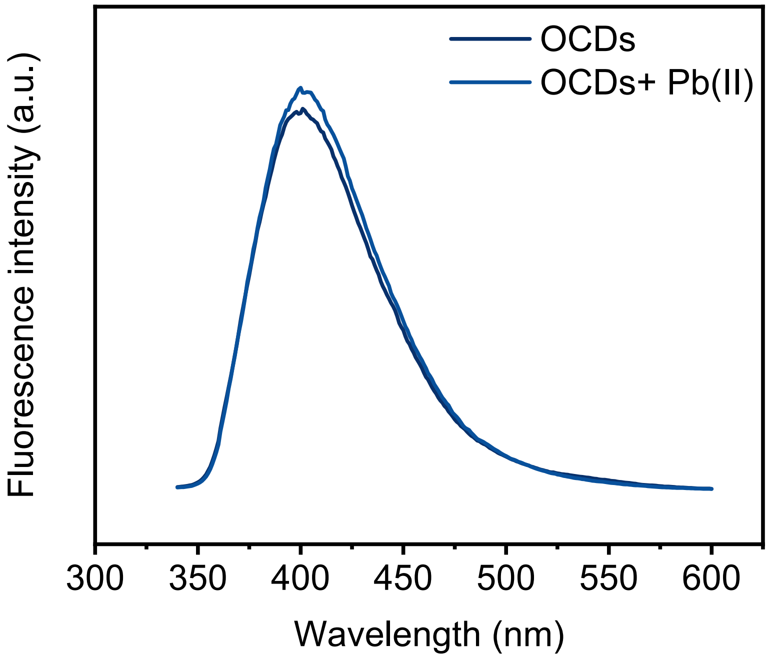


**Fig. S25** Fluorescence spectra of OCDs with and without Pb(II).

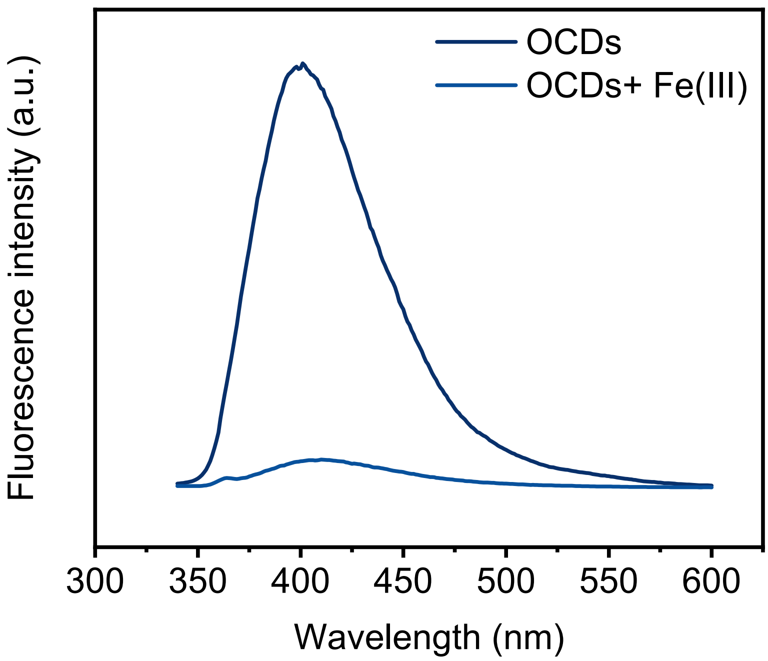


**Fig. S26** Fluorescence spectra of OCDs with and without Fe(III).

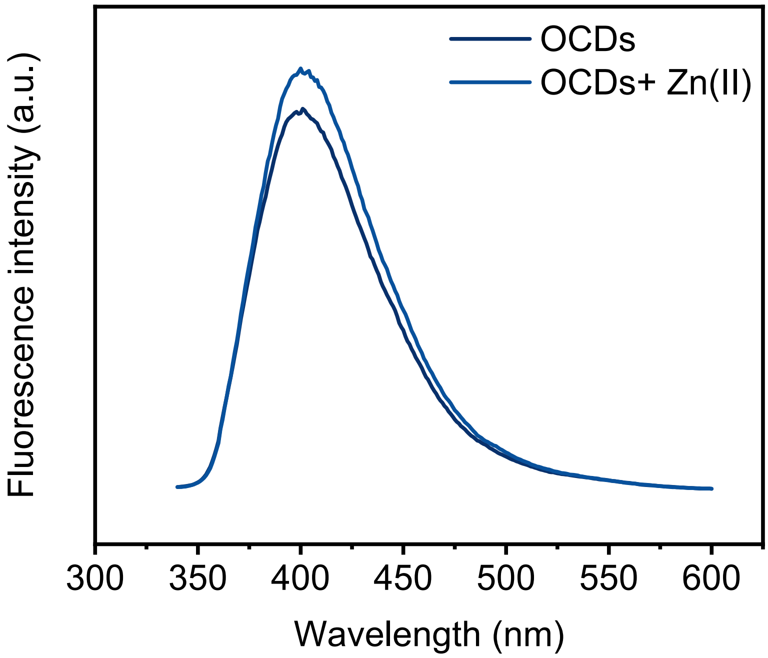


**Fig. S27** Fluorescence spectra of OCDs with and without Zn(II).

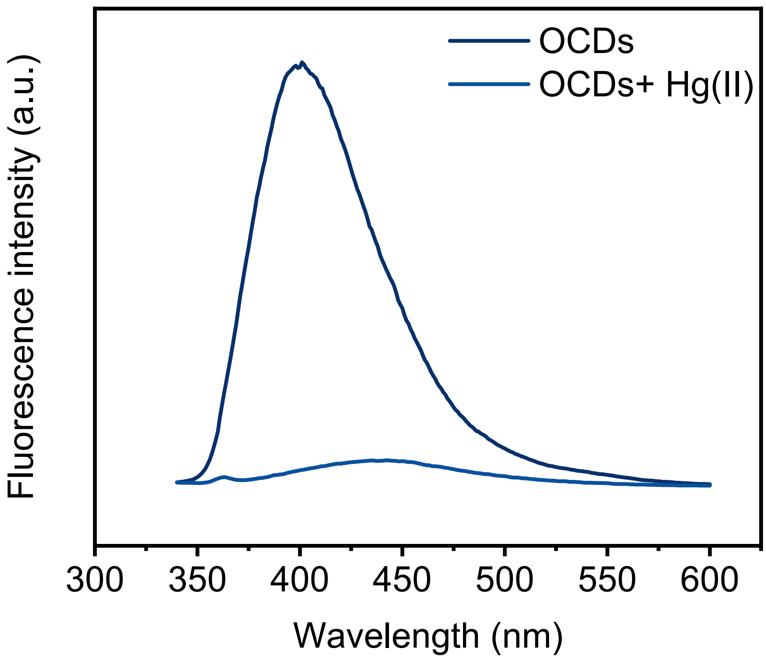


**Fig. S28** Fluorescence spectra of OCDs with and without Hg(II).

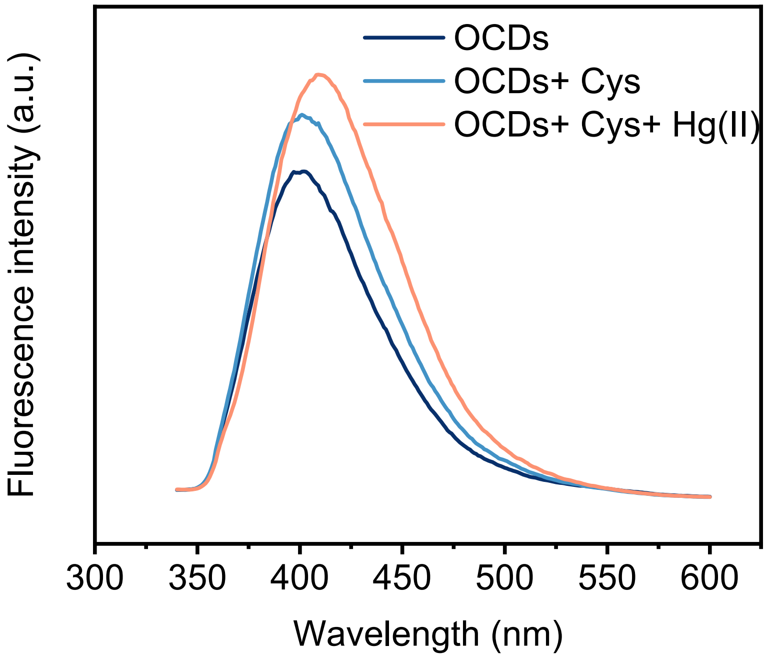


**Fig. S29** Comparison of fluorescence spectra of OCDs, OCDs + cysteine and OCDs + cysteine + Hg(II).

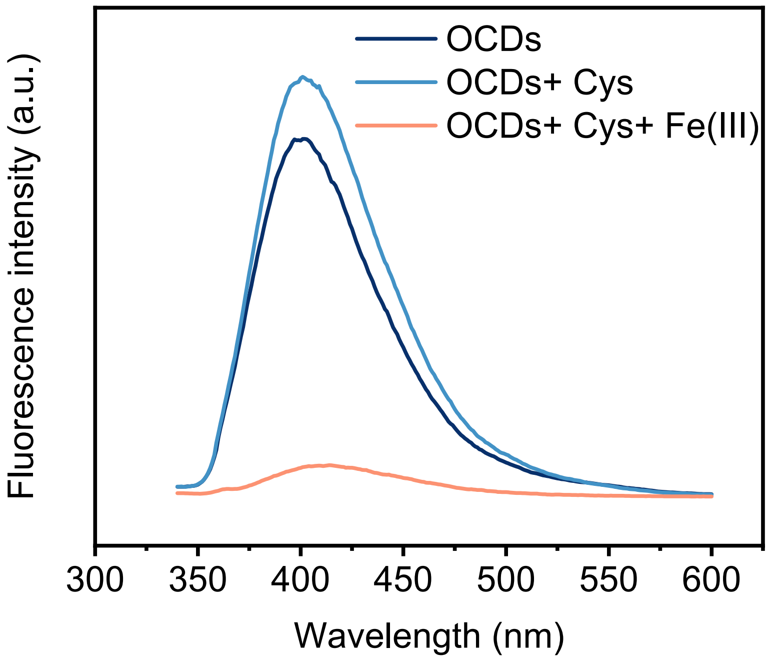


**Fig. S30** Comparison of fluorescence spectra of OCDs, OCDs + cysteine and OCDs + cysteine + Fe(III).

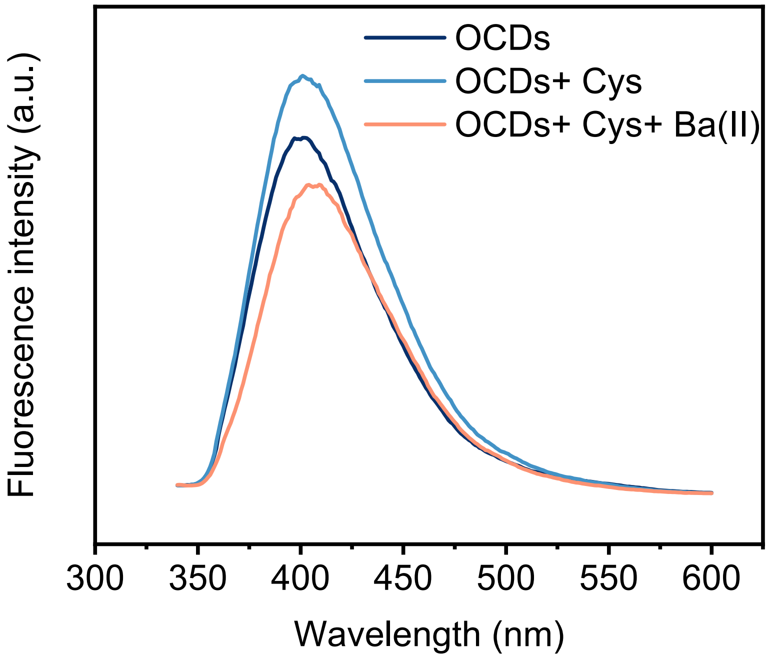


**Fig. S31** Comparison of fluorescence spectra of OCDs, OCDs + cysteine and OCDs + cysteine + Ba(II).

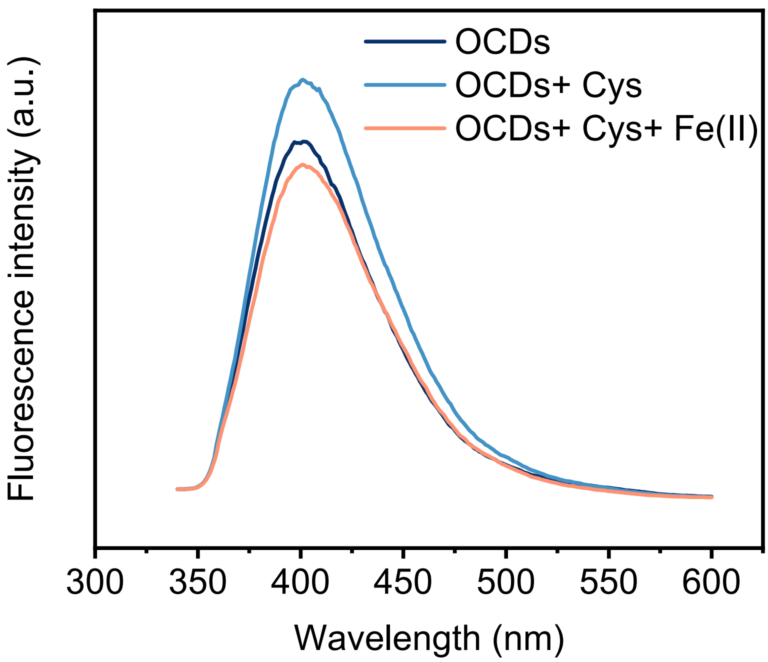


**Fig. S32** Comparison of fluorescence spectra of OCDs, OCDs + cysteine and OCDs + cysteine + Fe(II).

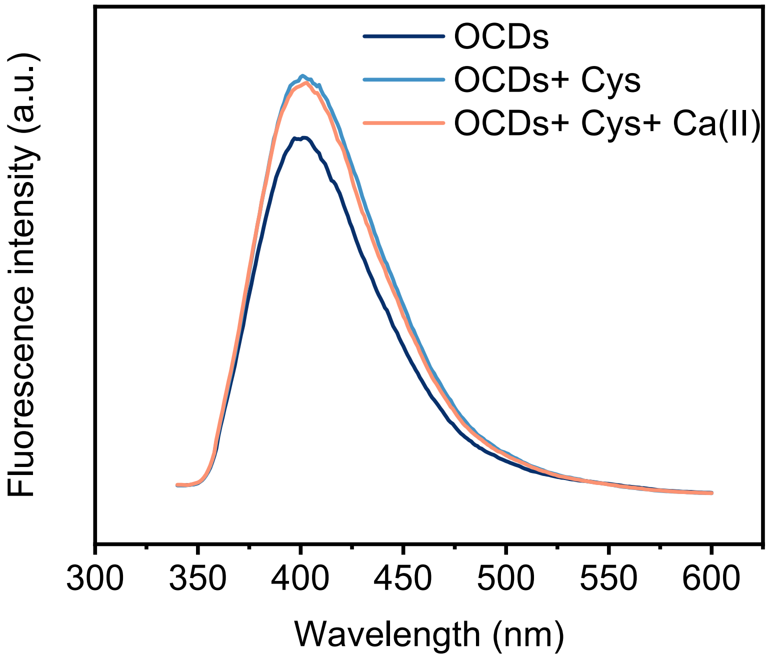


**Fig. S33** Comparison of fluorescence spectra of OCDs, OCDs + cysteine and OCDs + cysteine + Ca(II).

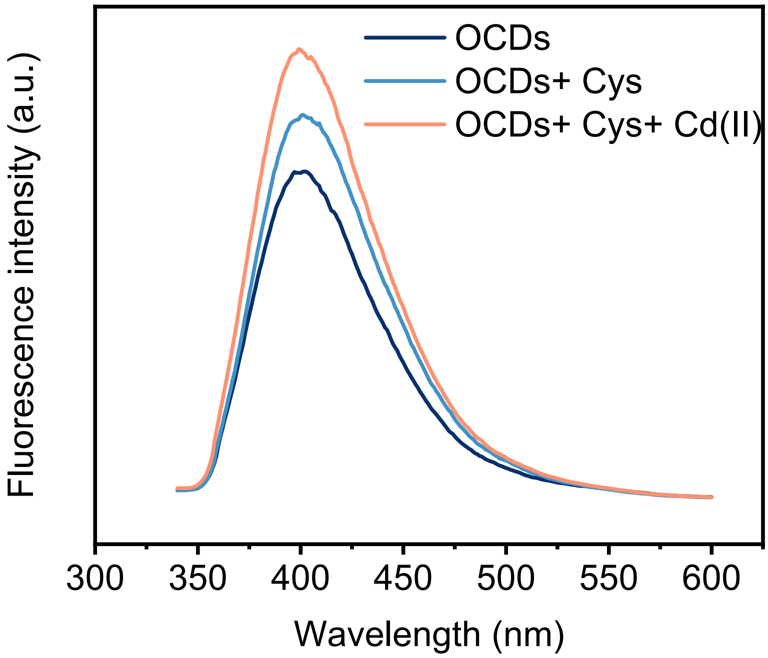


**Fig. S34** Comparison of fluorescence spectra of OCDs, OCDs + cysteine and OCDs + cysteine + Cd(II).

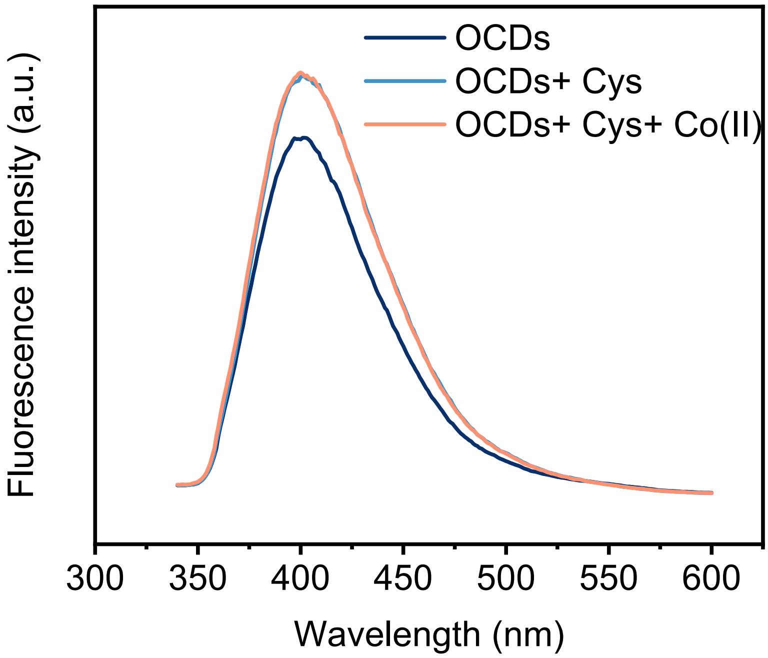


**Fig. S35** Comparison of fluorescence spectra of OCDs, OCDs + cysteine and OCDs + cysteine + Co(II).

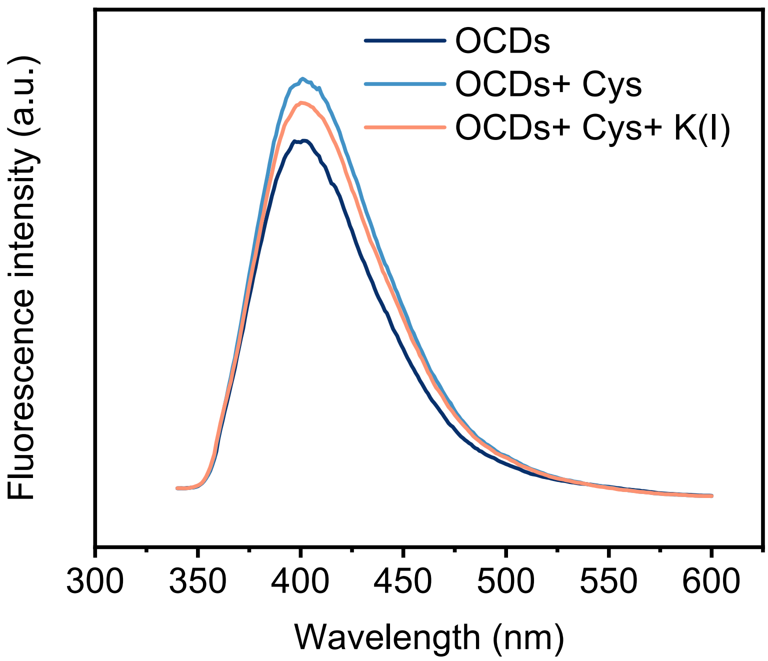


**Fig. S36** Comparison of fluorescence spectra of OCDs, OCDs + cysteine and OCDs + cysteine + K(I).

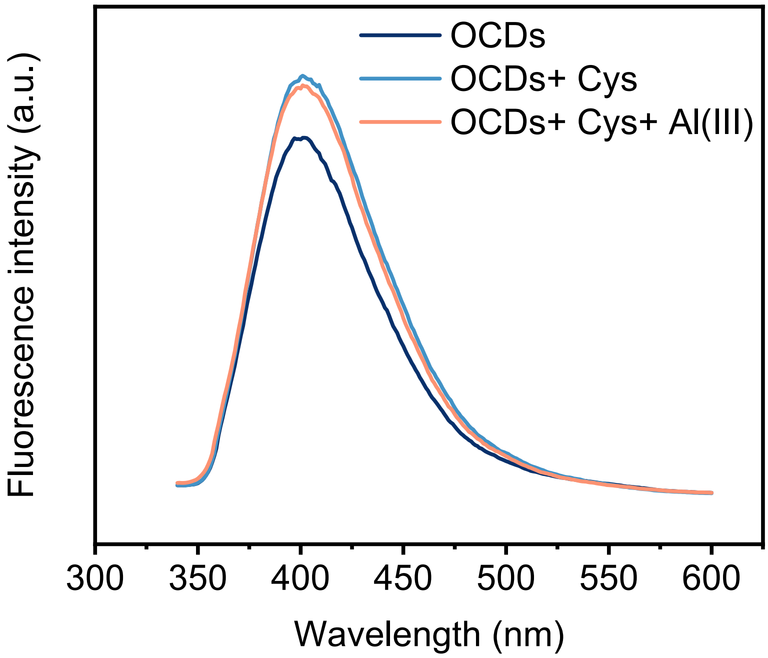


**Fig. S37** Comparison of fluorescence spectra of OCDs, OCDs + cysteine and OCDs + cysteine + Al(II).

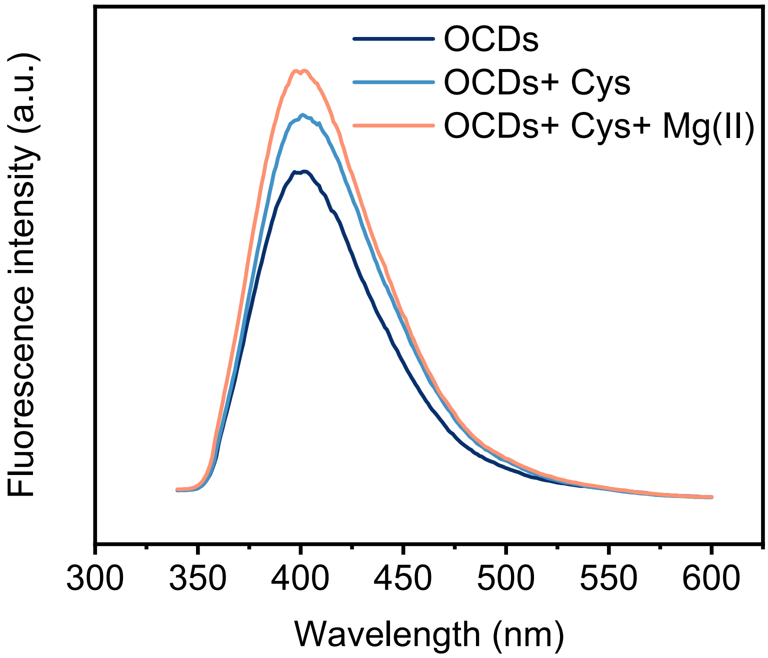


**Fig. S38** Comparison of fluorescence spectra of OCDs, OCDs + cysteine and OCDs + cysteine + Mg(II).

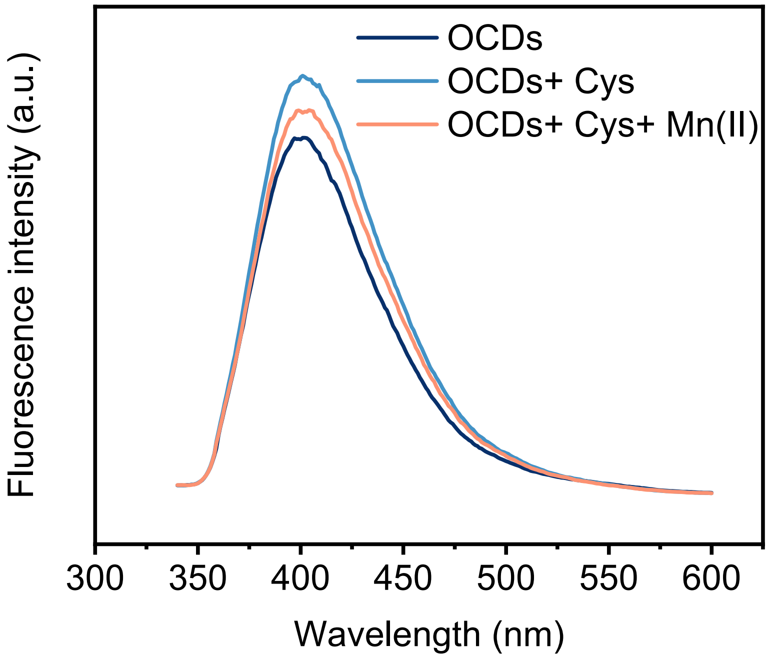


**Fig. S39** Comparison of fluorescence spectra of OCDs, OCDs + cysteine and OCDs + cysteine + Mn(II).

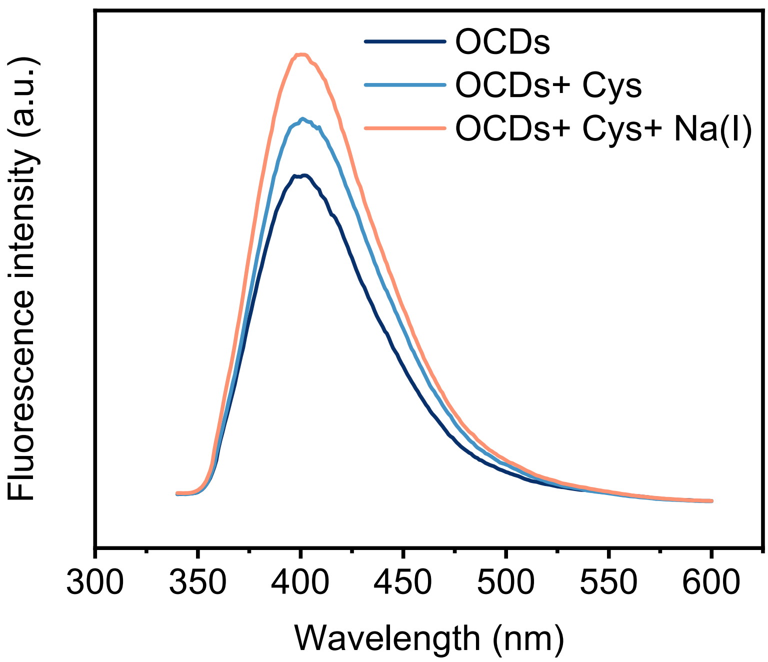


**Fig. S40** Comparison of fluorescence spectra of OCDs, OCDs + cysteine and OCDs + cysteine + Na(II).

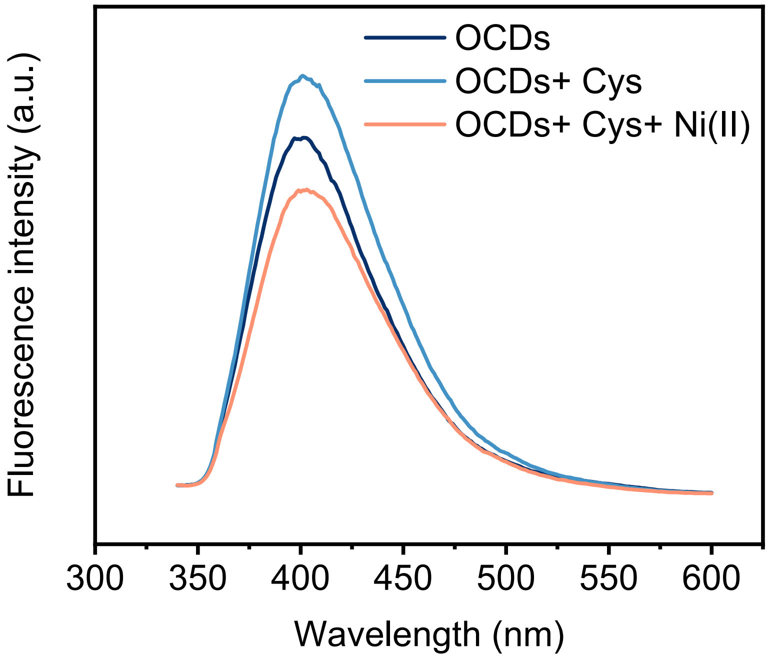


**Fig. S41** Comparison of fluorescence spectra of OCDs, OCDs + cysteine and OCDs + cysteine + Ni(II).

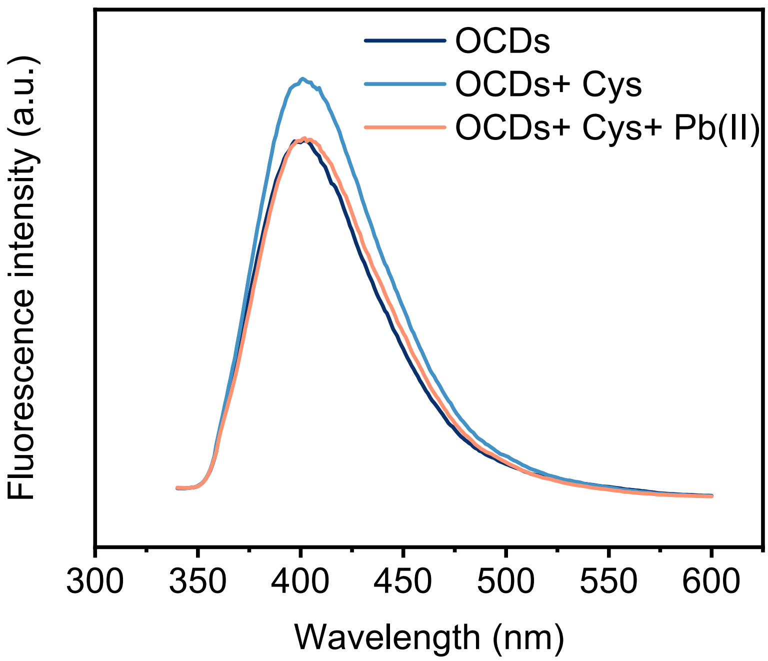


**Fig. S42** Comparison of fluorescence spectra of OCDs, OCDs + cysteine and OCDs + cysteine + Pb(II).

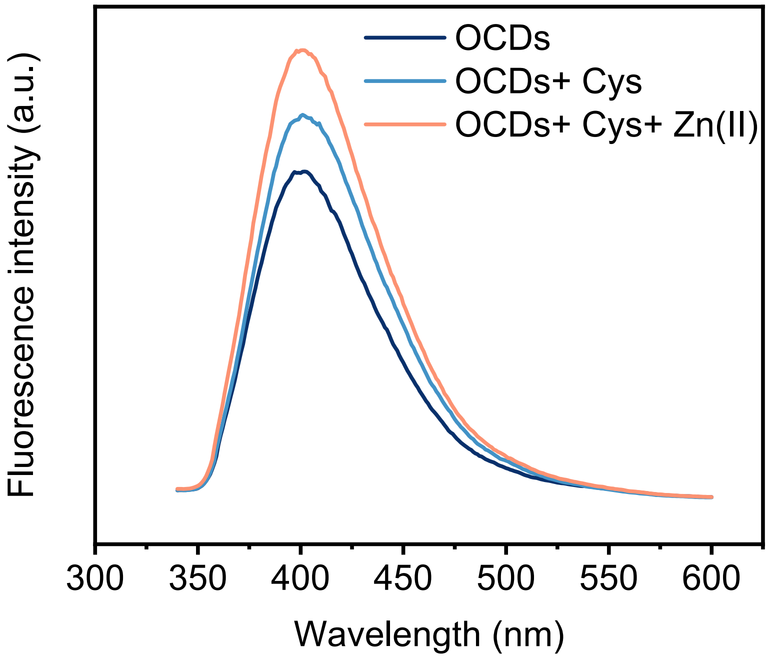


**Fig. S43** Comparison of fluorescence spectra of OCDs, OCDs + cysteine and OCDs + cysteine + Zn(II).

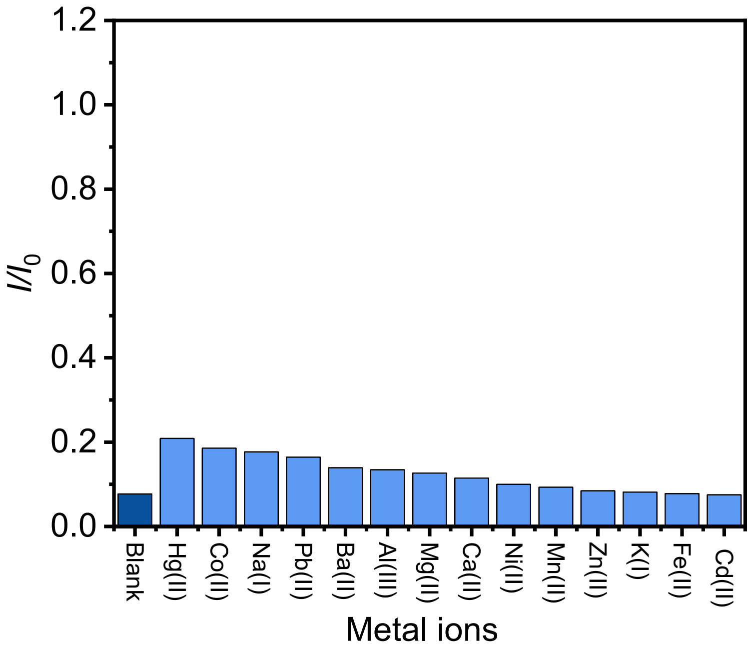


**Fig. S44** The comparison of relative fluorescence intensities of the mixtures of OCD, cysteine (0.3 mM) and Fe(III) (0.1 mM) with different metal ions.

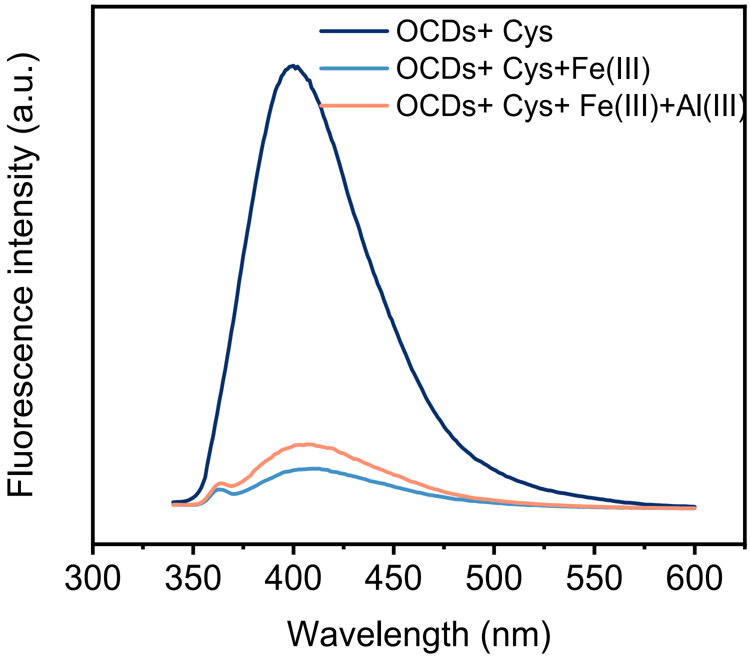


**Fig. S45** Comparison of fluorescence spectra of OCDs + cysteine, OCDs + cysteine + Fe(III) and OCDs + cysteine + Fe(III) + Al(III).

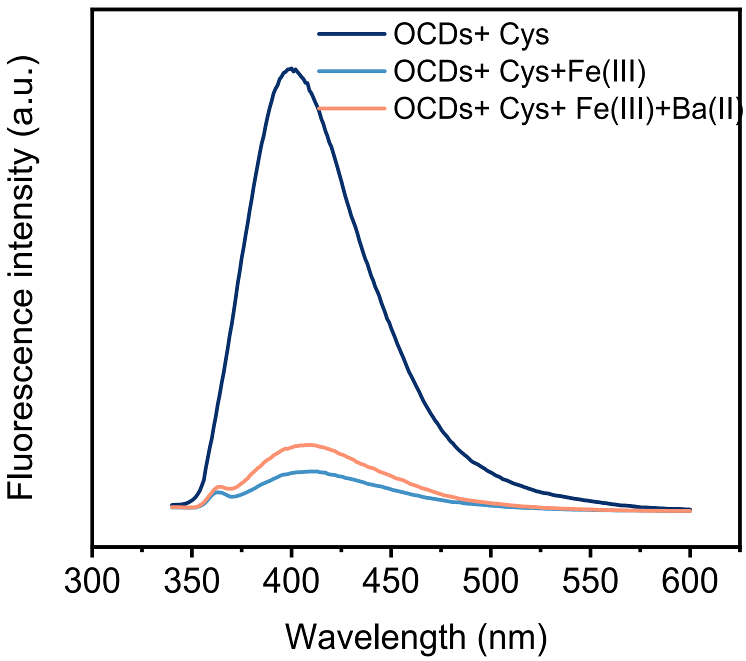


**Fig. S46** Comparison of fluorescence spectra of OCDs + cysteine, OCDs + cysteine + Fe(III) and OCDs + cysteine + Fe(III) + Ba(II).

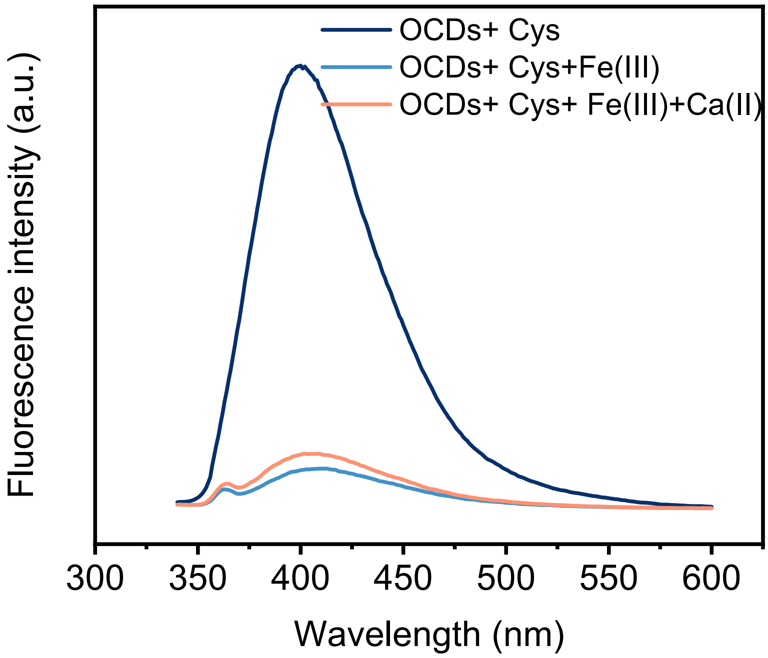


**Fig. S47** Comparison of fluorescence spectra of OCDs + cysteine, OCDs + cysteine + Fe(III) and OCDs + cysteine + Fe(III) + Ca(II).

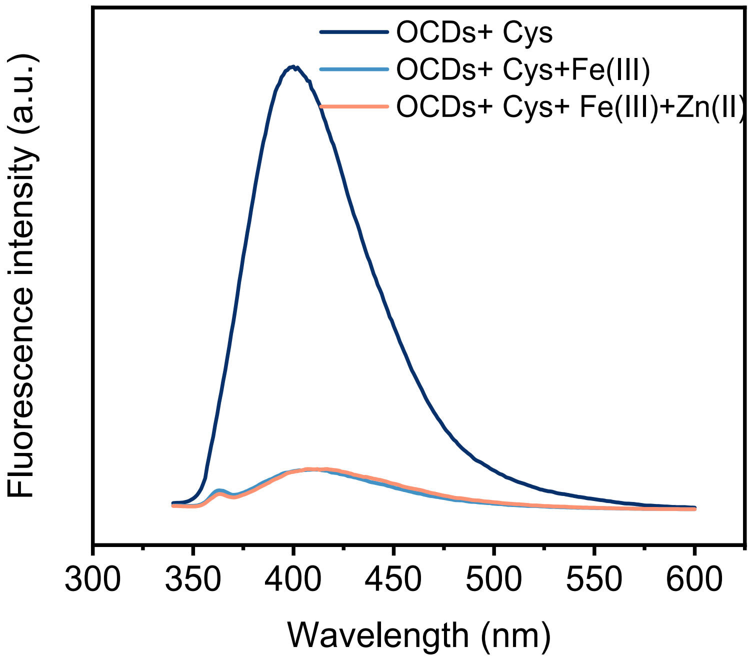


**Fig. S48** Comparison of fluorescence spectra of OCDs + cysteine, OCDs + cysteine + Fe(III) and OCDs + cysteine + Fe(III) + Zn(II).

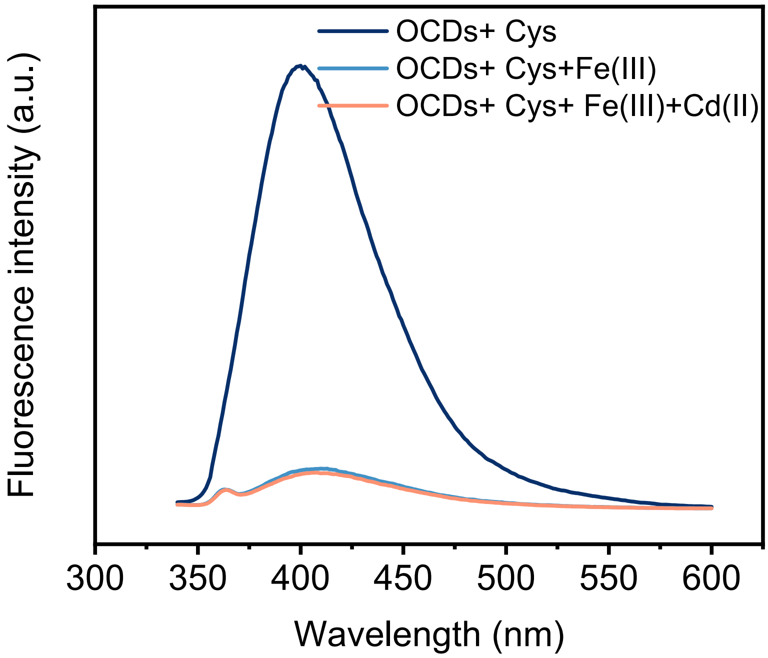


**Fig. S49** Comparison of fluorescence spectra of OCDs + cysteine, OCDs + cysteine + Fe(III) and OCDs + cysteine + Fe(III) + Cd(II).

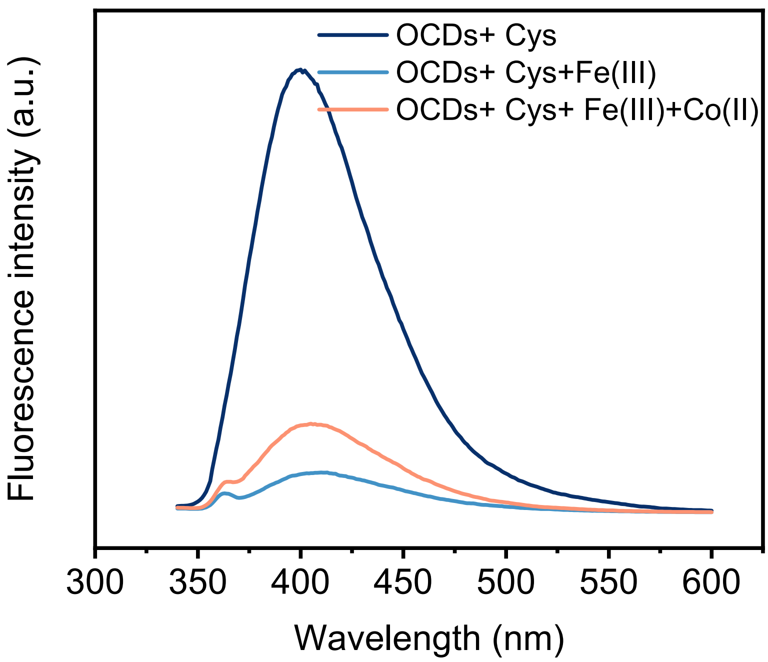


**Fig. S50** Comparison of fluorescence spectra of OCDs + cysteine, OCDs + cysteine + Fe(III) and OCDs + cysteine + Fe(III) +Co(II).

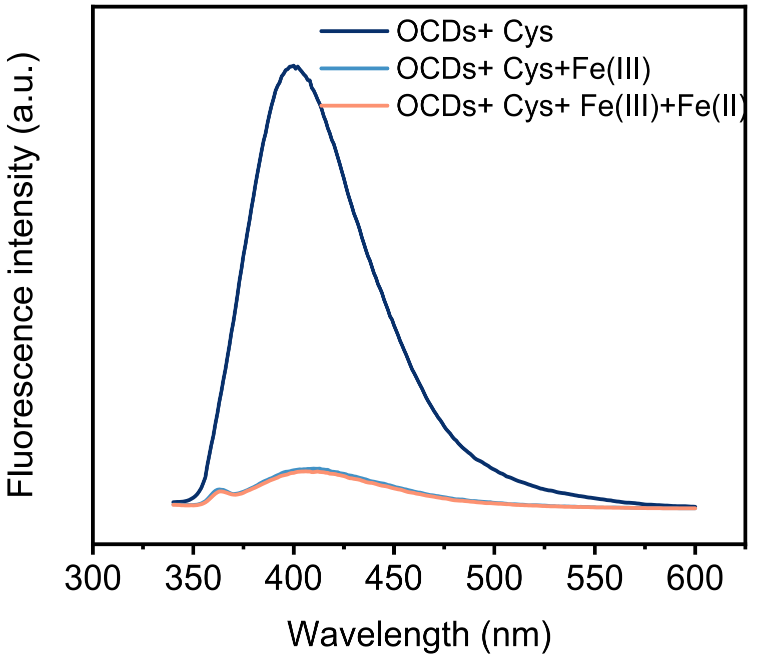


**Fig. S51** Comparison of fluorescence spectra of OCDs + cysteine, OCDs + cysteine + Fe(III) and OCDs + cysteine + Fe(III) + Fe(II).

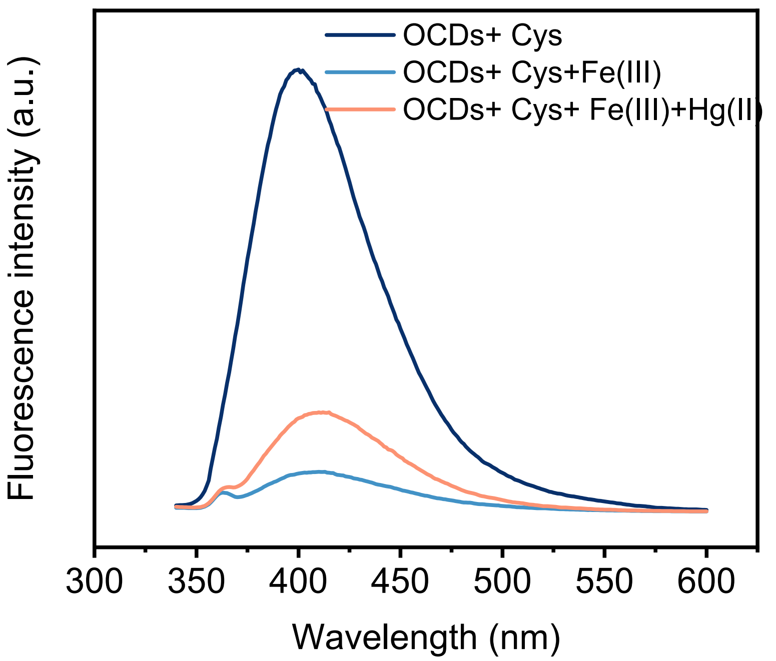


**Fig. S52** Comparison of fluorescence spectra of OCDs + cysteine, OCDs + cysteine + Fe(III) and OCDs + cysteine + Fe(III) + Hg(II).

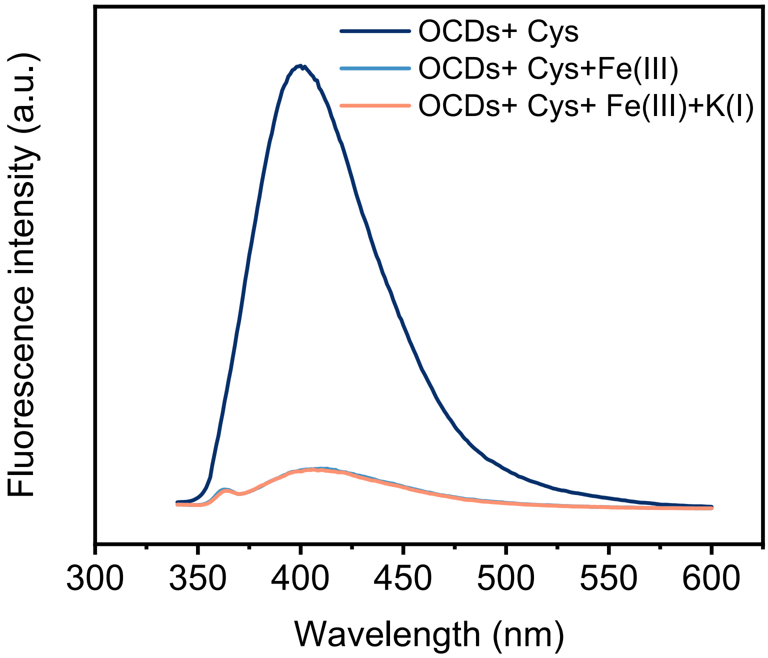


**Fig. S53** Comparison of fluorescence spectra of OCDs + cysteine, OCDs + cysteine + Fe(III) and OCDs + cysteine + Fe(III) + K(I).

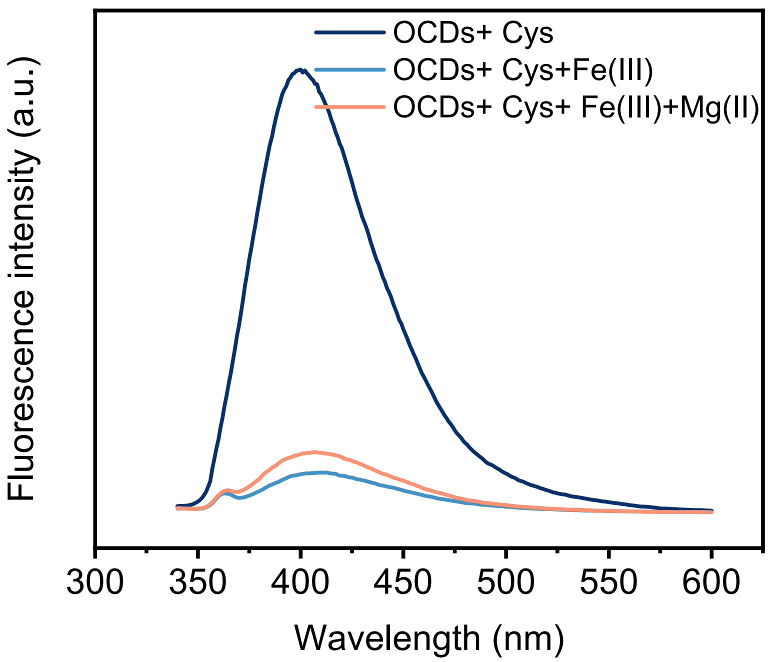


**Fig. S54** Comparison of fluorescence spectra of OCDs + cysteine, OCDs + cysteine + Fe(III) and OCDs + cysteine + Fe(III) + Mg(II).

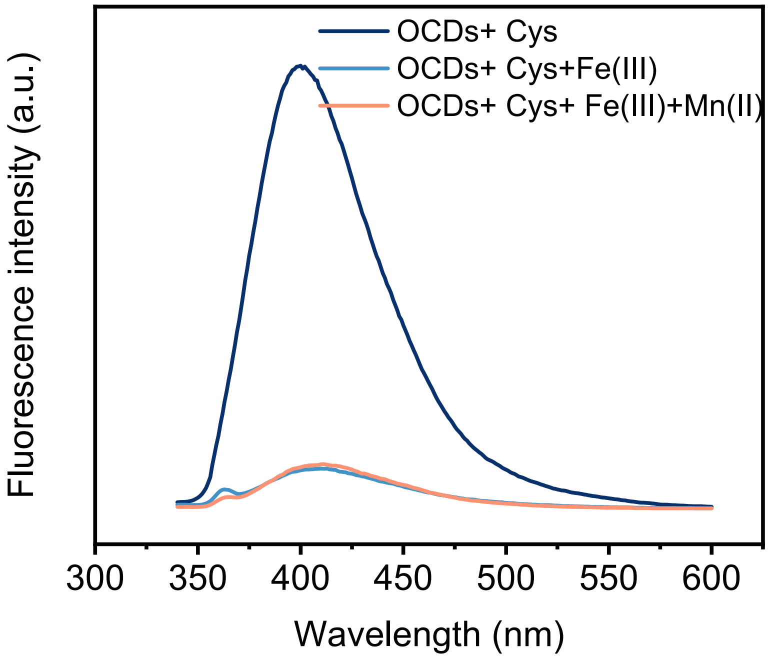


**Fig. S55** Comparison of fluorescence spectra of OCDs + cysteine, OCDs + cysteine + Fe(III) and OCDs + cysteine + Fe(III) + Mn(II).

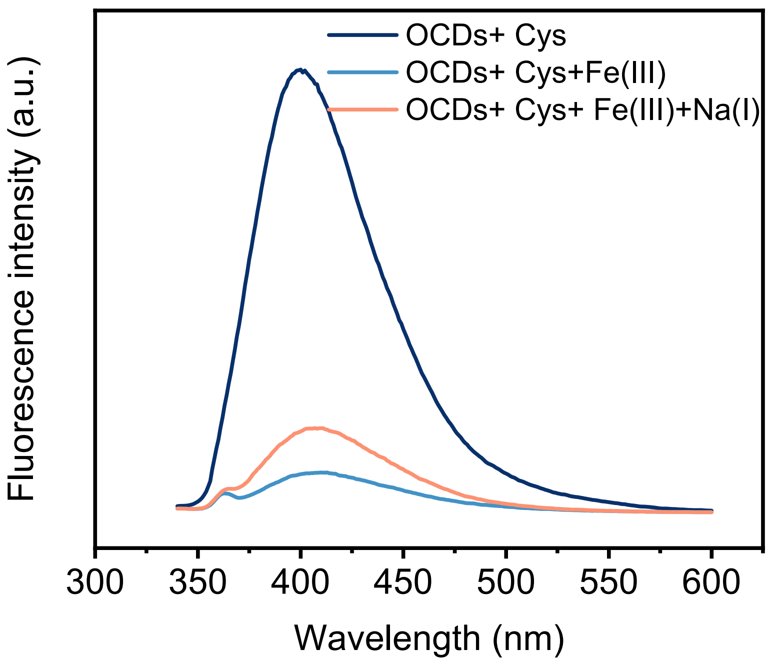


**Fig. S56** Comparison of fluorescence spectra of OCDs + cysteine, OCDs + cysteine + Fe(III) and OCDs + cysteine + Fe(III) + Na(I).

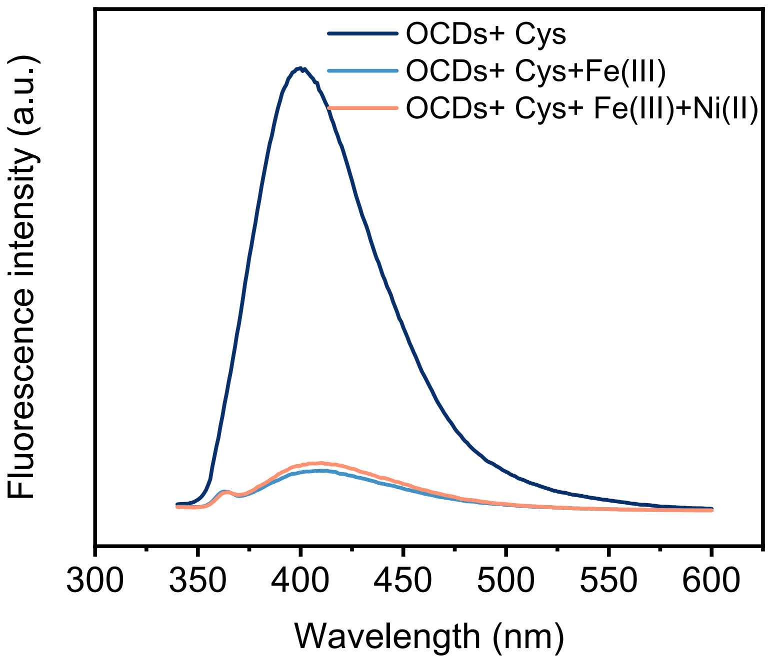


**Fig. S57** Comparison of fluorescence spectra of OCDs + cysteine, OCDs + cysteine + Fe(III) and OCDs + cysteine + Fe(III) + Ni(II).

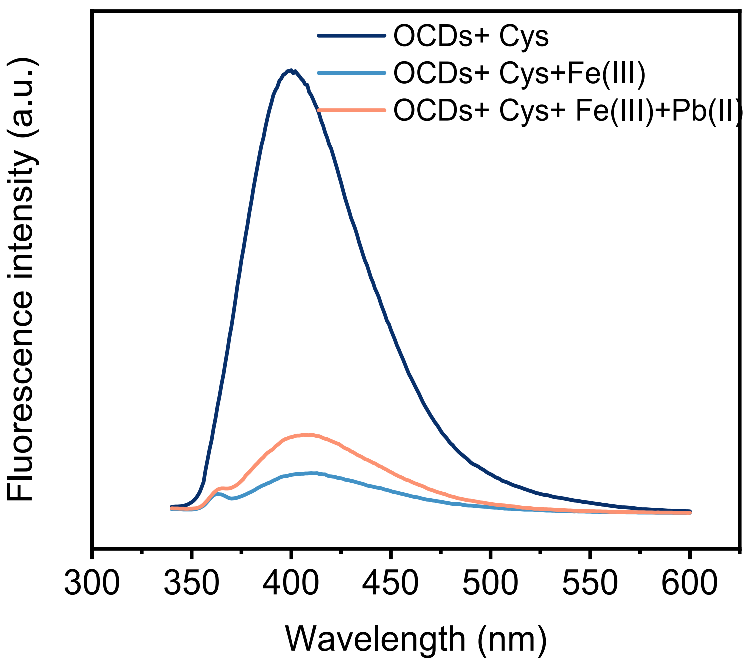


**Fig. S58** Comparison of fluorescence spectra of OCDs + cysteine, OCDs + cysteine + Fe(III) and OCDs + cysteine + Fe(III) + Pb(II).

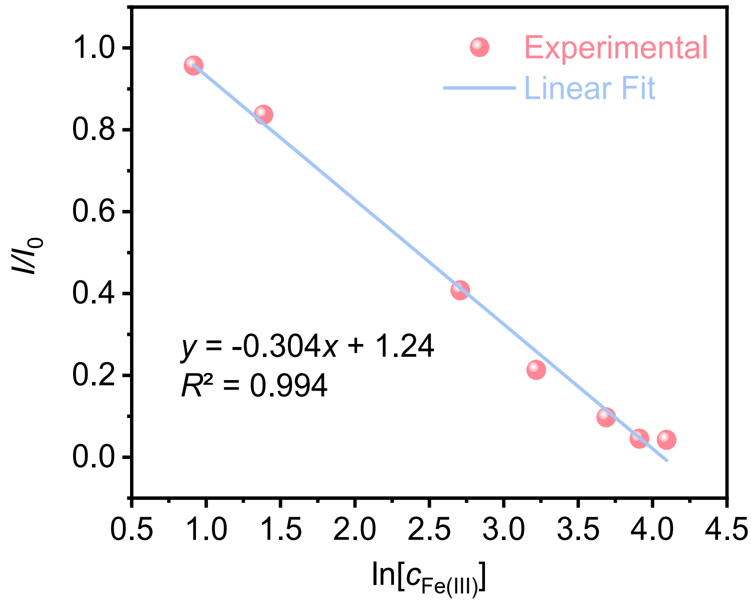


**Fig. S59** The linear relationship between ln[$c_{Fe(III)}$] and fluorescence intensity in real samples.

**Table S1.** Comparison of reaction conditions for preparing carbon dots (bottom-up) that can specifically detect $Fe^{3+}$.

| Materials | Precursor | Synthesis Methods | Reaction condition | References |
|---|---|---|---|---|
| BNCDs | 1,1′ -binaphthyl-2,2′ - diamine, citric acid and toluene | Hydrothermal | 180℃, 12 hours | Sens. Actuators B Chem. 2022, 360, 131645. |
| G-CDs | citric acid and melamine | Solvothermal | 180℃, 8 hours | Sens. Actuators B Chem. 2021, 342, 129963. |
| NCQDs | Tartaric acid and L-arginine | Solvothermal | 180℃, 12 hours | Microchem. J. 2020, 158, 105142. |
| S-doped C-dots | sodium citrate and sodium thiosulfate | Hydrothermal | 200℃, 6 hours | J. Mater. Chem. A 2015, 3 (2), 542-546. |
| C-dots | 4-Chlorophenol | Solvothermal | 185℃, 10 hours | Spectrochim. Acta. A Mol. Biomol. Spectrosc. 2020, 226, 117594. |
| OCDs | Oxytetracycline | Hydrothermal | 180℃, 1 hour | This work |

**Table S2.** Performance comparison of the as-prepared OCDs with other reported fluorescent switching-off CDs on Fe(III) detection, which are listed according to the order of sensitivity decreasing (The numbers in the table correspond to the numbers in **Fig. 4.c**).

| Number | Materials | Precursors | Method | Linear range (μM) | LOD (μM) | Sensitivity based on QE ($\mu M^{-1}$) | References |
|---|---|---|---|---|---|---|---|
| **1** | **OCDs** | **Oxytetracycline** | **bottom-up** | **0.5–20** | **0.440** | **$3.52\times10^{-2}$** | **This work.** |
| 2 | P,Cl-CDs | Maltose, phosphoric and hydrochloric acids | bottom-up | 0.1–8.0 | 0.060 | $5.67\times10^{-2}$ | S1 |
| 3 | La-CDs | Citric acid monohydrate, methylamine hydrochloride and lanthanum chloride heptahydrate | bottom-up | 0.15-10 | 0.091 | $3.361\times10^{-2}$ | S2 |
| 4 | C-dots | 4-Chlorophenol | bottom-up | 0.6–25 | 0.36 | $2.86\times10^{-2}$ | S3 |
| 5 | N-CDs | citric acid and allylamine hydrochloride | bottom-up | 0.05–30 | 0.0135 | $1.93\times10^{-2}$ | S4 |
| 6 | BNCDs | 1,1′-binaphthyl-2,2′-diamine, citric acid and toluene | bottom-up | 0-80 | 0.219 | $1.43\times10^{-2}$ | S5 |
| 7 | P95-CDs | Citric acid and phenylalanine | bottom-up | 0-50 | 3.5 | $1.03\times10^{-2}$ | S6 |
| 8 | N-CDs | citric acid and benzoylurea | bottom-up | 30–100 | 1.1 | $9.7\times10^{-3}$ | S7 |
| 9 | G-CDs | citric acid and melamine | bottom- | 0.5-50 | 0.1 | $7.7\times10^{-3}$ | S8 |

| | | | | | | | |
|---|---|---|---|---|---|---|---|
| | | | up | | | | |
| 10 | EfCDs | Acrylamide,EDTA and Ammonium persulfate | bottom-up | 0-50 | 0.0338 | $7×10^{−3}$ | S9 |
| 11 | Carbon dots | L-glutamic acid and anhydrous ethylenediamine | bottom-up | 8–80 | 3.8 | $3.58×10^{−3}$ | S10 |
| 12 | HCDs | Citric acid,branched polyethyleneimine and potassium thiocyanate | bottom-up | 1-150 | 0.052 | $3.3×10^{−3}$ | S11 |
| 13 | NCQDs | Tartaric acid and *L*-arginine | bottom-up | 0–70 | 0.50 | $3.13×10^{−3}$ | S12 |
| 14 | CDs-1 | p-Benzoquinone and EDA | bottom-up | 25-200 | 22 | $2.7×10^{−3}$ | S13 |
| 15 | Ph-gCNQDs | Citric acid, urea, dipotassium hydrogen phosphate and oleic acid. | bottom-up | 0–250 | 25.18 | $2.54×10^{−3}$ | S14 |
| 16 | B, N-CDs | Citric acid, tris base and boric acid | bottom-up | 0–400 | 5.36 | $2.28×10^{−3}$ | S15 |
| 17 | S-doped C-dots | sodium citrate and sodium thiosulfate | bottom-up | 1–500 | 0.1 | $2.01×10^{−3}$ | S16 |
| 18 | CDs | p-dihydroxybenzene and EDA | bottom-up | 0-150 | 0.039 | $2×10^{−3}$ | S17 |
| 19 | CDs | glycerol and DAMO | bottom-up | 0.1-100 | 0.016 | $1.48×10^{−3}$ | S18 |
| 20 | CQDs | Citric acid and 1-aminopropyl-3-methylimidazolium | bottom-up | 0–300 | 13.68 | $1.27×10^{−3}$ | S19 |
| 21 | E-CNDs | Ethylenediamine | bottom-up | 0.5–2000 | 0.018 | $4.76×10^{−4}$ | S20 |

| | | | | | | | |
|---|---|---|---|---|---|---|---|
| 22 | CQDs | *Catharanthus* roseus | top-down | 1–6 | 0.8 | $2.99\times10^{-2}$ | S21 |
| 23 | C-dots | *Curauá*-fiber | top-down | 0–30 | 0.77 | $2.42\times10^{-2}$ | S22 |
| 24 | CDs | citric acid,polyvinylpyrrolidone and methionine | bottom-up | 0-1000 | 0.00026 | $1.295\times10^{-2}$ | S23 |
| 25 | CQDs | Pear juice | top-down | 0–50 | 2.28 | $1.22\times10^{-2}$ | S24 |
| 26 | HN-CDs | dwarf banana peel | top-down | 5-25 | 0.66 | $9.1\times10^{-3}$ | S25 |
| 27 | N-CDs | *Magnolia liliiflora* flower | top-down | 1–25 | 1.2 | $6.83\times10^{-3}$ | S26 |
| 28 | N-CDs | soluble starch and EDA | top-down | 0-80 | 0.0849 | $6.2\times10^{-3}$ | S27 |
| 29 | N-CDs | natural bauhinia flflower | top-down | 0-350 | 0.01 | $6.2\times10^{-3}$ | S28 |
| 30 | KCDs | kerosene fuel soot | top-down | 0-150 | 2.25 | $6\times10^{-3}$ | S29 |
| 31 | CDs | Polymeric reverse osmosis (RO) membranes and $H_2O_2$ | top-down | 0-100 | 2.97 | $5.3\times10^{-3}$ | S30 |
| 32 | NGQDs | chitosan and different acids | top-down | 0-300 | 0.0667 | $4.5\times10^{-3}$ | S31 |
| 33 | CDs | Chloroplasts of spinach | top-down | 1.0–100.0 | 0.3 | $3.78\times10^{-3}$ | S32 |
| 34 | CDs | Sweet *potato* | top-down | 1–100 | 0.32 | $3.7\times10^{-3}$ | S33 |
| 35 | FNCDs | *Phyllanthus acidus* and aqueous ammonia | top-down | 2-25 | 0.9 | $3.4\times10^{-3}$ | S34 |
| 36 | CDs | charcoal | top-down | 50-250 | 72 | $3\times10^{-3}$ | S35 |
| 37 | S,N-doped C-dots | Distillers dried solubles | top-down | 0.01–16 | 0.0032 | $2.72\times10^{-3}$ | S36 |
| 38 | N,S-CDs | chitosan and κ-carr | top-down | 1-100 | 0.057 | $2.69\times10^{-3}$ | S37 |
| 39 | CNs | Pith of *tapioca* | top-down | 20–200 | 26.5 | $2.59\times10^{-3}$ | S38 |
| 40 | CNDs | Olive solid wastes | top-down | 0-50 | 1.4 | $2.4\times10^{-3}$ | S39 |
| 41 | CD-CP | Chlorella pyrenoidosa | top-down | 1.6-200 | 0.00055 | $2.2\times10^{-3}$ | S40 |
| 42 | GQDs | alkali lignin | top-down | 0-500 | 1.49 | $1.3\times10^{-3}$ | S41 |

| | | | | | | | |
|---|---|---|---|---|---|---|---|
| 43 | MCDs | Ganoderma lucidum spores | top-down | 0.0025-0.1 | 0.0159 | $1.3\times10^{-3}$ | S42 |
| 44 | P-CQDs | pine wood | top-down | 0-2000 | 0.3554 | $1.1\times10^{-3}$ | S43 |
| 45 | CB-CDs | *Cranberry* beans | top-down | 30–600 | 9.55 | $9.65\times10^{-4}$ | S44 |
| 46 | M-GQDs | Miscanthus and p-amino-benzenesulfonic acid monosodium salt | top-down | 0-1000 | 0.00141 | $2.94\times10^{-4}$ | S45 |
| 47 | CA-CFCDs | spent coffee grounds and citric acid | top-down | 0-200 | 2.25 | $1.74\times10^{-4}$ | S46 |

**Table S3.** Detection of $Fe^{3+}$ in actual water samples.

| Samples | Added (μM) | Measured (μM) | Recovery (%) | RSD (%) |
|---|---|---|---|---|
| Lake water | 2.5 | 2.29 | 91.6 | 0.69 |
| | 4 | 3.50 | 87.5 | 0.52 |
| | 15 | 15.84 | 105.6 | 0.39 |
| | 40 | 47.22 | 118.1 | 1.63 |
| | 50 | 56.83 | 113.7 | 1.46 |
| | 60 | 57.35 | 95.6 | 1.80 |

## References

S1. Wang, W.; Peng, J.; Li, F.; Su, B.; Chen, X.; Chen, X., Phosphorus and Chlorine Co-Doped Carbon Dots with Strong Photoluminescence as a Fluorescent Probe for Ferric Ions. *Microchim. Acta* **2018,** *186* (1), 32.

S2. Yang, S.; Sun, X.; Wang, Z.; Wang, X.; Guo, G.; Pu, Q., Anomalous Enhancement of Fluorescence of Carbon Dots through Lanthanum Doping and Potential Application in Intracellular Imaging of Ferric Ion. *Nano Res.* **2018,** *11* (3), 1369-1378.

S3. Wang, Y.; Man, Y.; Li, S.; Wu, S.; Zhao, X.; Xie, F.; Qu, Q.; Zou, W.-S., Pesticide-Derived Bright Chlorine-Doped Carbon Dots for Selective Determination and Intracellular Imaging of Fe(III). *Spectrochim. Acta. A Mol. Biomol. Spectrosc.* **2020,** *226*, 117594.

S4. Zhou, X.; Zhao, G.; Tan, X.; Qian, X.; Zhang, T.; Gui, J.; Yang, L.; Xie, X., Nitrogen-Doped Carbon Dots with High Quantum Yield for Colorimetric and Fluorometric Detection of Ferric Ions and in a Fluorescent Ink. *Microchim. Acta* **2019,** *186* (2), 67.

S5. Wang, W.; Wu, J.; Xing, Y.; Wang, Z., Solvent-Dependent Red Emissive Carbon Dots and Their Applications in Sensing and Solid-State Luminescence. *Sens. Actuators B Chem.* **2022,** *360,* 131645.

S6. Chahal, S.; Yousefi, N.; Tufenkji, N., Green Synthesis of High Quantum Yield Carbon Dots from Phenylalanine and Citric Acid: Role of Stoichiometry and Nitrogen Doping. *ACS Sustain. Chem. Eng.* **2020,** *8* (14), 5566-5575.

S7. Shan, F.; Xia, H.; Xie, X.; Fu, L.; Yang, H.; Zhou, Q.; Zhang, Y.; Wang, Z.; Yu, X., Novel N-Doped Carbon Dots Prepared Via Citric Acid and Benzoylurea by Green Synthesis for High Selectivity Fe(III) Sensing and Imaging in Living Cells. *Microchem. J.* **2021,** *167*, 106273.

S8. Liu, G.; Kong, D.; Han, J.; Zhou, R.; Gao, Y.; Wu, Z.; Zhao, L.; Wang, C.; Wang, L.; Lu, G., Solvent-Controlled Synthesis of Full-Color Carbon Dots and Its Application as a Fluorescent Food-Tasting Sensor for Specific Recognition of Jujube Species. *Sens. Actuators B Chem.* **2021,** *342,* 129963.

S9. Dong, J.; Li, B.; Xiao, J.; Liu, G.; Baulin, V.; Feng, Y.; Jia, D.; Tsivadze, A. Y.; Zhou, Y., Carbon Dots with Tailor-Made Chelating Ligands for Specific Metal Ions Recognition: Target Synthesis and Prediction of Metal Ions Selectivity. *Carbon* **2022,** *199*, 151-160.

S10. Chen, Y.; Sun, X.; Pan, W.; Yu, G.; Wang, J., $Fe^{3+}$-Sensitive Carbon Dots for Detection of $Fe^{3+}$ in Aqueous Solution and Intracellular Imaging of $Fe^{3+}$ inside Fungal Cells. *Front. Chem.* **2020,** *7*.

S11. Shi, Y.; Liu, J.; Zhang, Y.; Bao, J.; Cheng, J.; Yi, C., Microwave-Assisted Synthesis of Colorimetric and Fluorometric Dual-Functional Hybrid Carbon Nanodots for $Fe^{3+}$ Detection and Bioimaging. *Chin. Chem. Lett.* **2021,** *32* (10), 3189-3194.

S12. Zhu, J.; Chu, H.; Wang, T.; Wang, C.; Wei, Y., Fluorescent Probe Based Nitrogen Doped Carbon Quantum Dots with Solid-State Fluorescence for the Detection of $Hg^{2+}$ and $Fe^{3+}$ in Aqueous Solution. *Microchem. J.* **2020,** *158*, 105142.

S13. Hong, Q.; Wang, X.-Y.; Gao, Y.-T.; Lv, J.; Chen, B.-B.; Li, D.-W.; Qian, R.-C., Customized Carbon Dots with Predictable Optical Properties Synthesized at Room Temperature Guided by Machine Learning. *Chem. Mater.* **2022,** *34* (3), 998-1009.

S14. Vashisht, D.; Sharma, E.; Kaur, M.; Vashisht, A.; Mehta, S. K.; Singh, K., Solvothermal Assisted Phosphate Functionalized Graphitic Carbon Nitride Quantum Dots for Optical Sensing of Fe Ions and Its Thermodynamic Aspects. *Spectrochim. Acta. A Mol. Biomol. Spectrosc.* **2020,** *228*, 117773.

S25. Tummala, S.; Lee, C.-H.; Ho, Y.-P., Boron, and Nitrogen Co-Doped Carbon Dots as a Multiplexing Probe for Sensing of P-Nitrophenol, Fe (Iii), and Temperature. *Nanotechnol.* **2021,** *32* (26), 265502.

S16. Xu, Q.; Pu, P.; Zhao, J.; Dong, C.; Gao, C.; Chen, Y.; Chen, J.; Liu, Y.; Zhou, H., Preparation of Highly Photoluminescent Sulfur-Doped Carbon Dots for Fe(Iii) Detection. *J. Mater. Chem. A* **2015,** *3* (2), 542-546.

S17. Han, Y.; Tang, B.; Wang, L.; Bao, H.; Lu, Y.; Guan, C.; Zhang, L.; Le, M.; Liu, Z.; Wu, M., Machine-Learning-Driven Synthesis of Carbon Dots with Enhanced Quantum Yields. *ACS Nano* **2020,** *14* (11), 14761-14768.

S18. Gao, G.; Jiang, Y.-W.; Jia, H.-R.; Yang, J.; Wu, F.-G., On-Off-on Fluorescent Nanosensor for $Fe^{3+}$ Detection and Cancer/Normal Cell Differentiation Via Silicon-Doped Carbon Quantum Dots. *Carbon* **2018,** *134*, 232-243.

S19. Xie, Z.; Sun, X.; Jiao, J.; Xin, X., Ionic Liquid-Functionalized Carbon Quantum Dots as Fluorescent Probes for Sensitive and Selective Detection of Iron Ion and Ascorbic Acid. *Colloids Surf. A Physicochem. Eng. Aspects* **2017,** *529*, 38-44.

S20. Arvapalli, D. M.; Sheardy, A. T.; Alapati, K. C.; Wei, J., High Quantum Yield Fluorescent Carbon Nanodots for Detection of Fe (Iii) Ions and Electrochemical Study of Quenching Mechanism. *Talanta* **2020,** *209*, 120538.

S21. Arumugham, T.; Alagumuthu, M.; Amimodu, R. G.; Munusamy, S.; Iyer, S. K., A Sustainable Synthesis of Green Carbon Quantum Dot (Cqd) from Catharanthus Roseus (White Flowering Plant) Leaves and Investigation of Its Dual Fluorescence Responsive Behavior in Multi-Ion Detection and Biological Applications. *Sustain. Mater. Technol.* **2020,** *23*, e00138.

S22. Raja, S.; Buhl, E. M.; Dreschers, S.; Schalla, C.; Zenke, M.; Sechi, A.; Mattoso, L. H. C., Curauá-Derived Carbon Dots: Fluorescent Probes for Effective Fe(Iii) Ion Detection, Cellular Labeling and Bioimaging. *Mater. Sci. Eng. C* **2021,** *129*, 112409.

S23. Yang, Z.; Xu, T.; Zhang, S.; Li, H.; Ji, Y.; Jia, X.; Li, J., Multifunctional N,S-Doped and Methionine Functionalized Carbon Dots for on-Off-on Fe(3+) and Ascorbic Acid Sensing, Cell Imaging, and Fluorescent Ink Applying. *Nano Res.* **2022**, 1-11.

S24. Das, G. S.; Shim, J. P.; Bhatnagar, A.; Tripathi, K. M.; Kim, T., Biomass-Derived Carbon Quantum Dots for Visible-Light-Induced Photocatalysis and Label-Free Detection of Fe(Iii) and Ascorbic Acid. *Sci. Rep.* **2019,** *9* (1), 15084.

S25. Atchudan, R.; Edison, T. N. J. I.; Perumal, S.; Muthuchamy, N.; Lee, Y. R., Hydrophilic Nitrogen-Doped Carbon Dots from Biowaste Using Dwarf Banana Peel for Environmental and Biological Applications. *Fuel* **2020,** *275*.

S26. Atchudan, R.; Edison, T. N. J. I.; Aseer, K. R.; Perumal, S.; Lee, Y. R., Hydrothermal Conversion of Magnolia Liliiflora into Nitrogen-Doped Carbon Dots as an Effective Turn-Off Fluorescence Sensing, Multi-Colour Cell Imaging and Fluorescent Ink. *Colloids Surf. B Biointerfaces* **2018,** *169*, 321-328.

S27. Li, B.; Gong, D.; Li, X.; Zhang, L.; Dong, Y.; Li, W.; Liu, W.; Qin, W.; Wang, Y., Subcellular Fluorescence Imaging for Bhk Cell and Multiple Sensing Based on Carbon Dots with Two Strong Emission Peaks. *Sens. Actuators B Chem.* **2018,** *258*, 757-765.

S28. Huang, Q.; Li, Q.; Chen, Y.; Tong, L.; Lin, X.; Zhu, J.; Tong, Q., High Quantum Yield Nitrogen-Doped Carbon Dots: Green Synthesis and Application as "Off-on" Fluorescent Sensors for the Determination of $Fe^{3+}$ and Adenosine Triphosphate in Biological Samples. *Sens. Actuators B Chem.* **2018,** *276*, 82-88.

S29. Venkatesan, S.; Mariadoss, A. J.; Arunkumar, K.; Muthupandian, A., Fuel Waste to Fluorescent Carbon Dots and Its Multifarious Applications. *Sens. Actuators B Chem.* **2019,** *282*, 972-983.

S30. Liang, L.; Veksha, A.; Mohamed Amrad, M. Z. B.; Snyder, S. A.; Lisak, G., Upcycling of Exhausted Reverse Osmosis Membranes into Value-Added Pyrolysis Products and Carbon Dots. *J. Hazard Mater.* **2021,** *419*, 126472.

S31. Kurniawan, D.; Weng, R.-J.; Setiawan, O.; Ostrikov, K.; Chiang, W.-H., Microplasma Nanoengineering of Emission-Tuneable Colloidal Nitrogen-Doped Graphene Quantum Dots as Smart Environmental-Responsive Nanosensors and Nanothermometers. *Carbon* **2021,** *185*, 501-513.

S32. Ran, Y.; Wang, S.; Yin, Q.; Wen, A.; Peng, X.; Long, Y.; Chen, S., Green Synthesis of Fluorescent Carbon Dots Using Chloroplast Dispersions as Precursors and Application for $Fe^{3+}$ Ion Sensing. *Luminescence* **2020,** *35* (6), 870-876.

S33. Shen, J.; Shang, S.; Chen, X.; Wang, D.; Cai, Y., Facile Synthesis of Fluorescence Carbon Dots from Sweet Potato for $Fe^{3+}$ Sensing and Cell Imaging. *Mater. Sci. Eng. C* **2017,** *76*, 856-864.

S34. Atchudan, R.; Edison, T. N. J. I.; Aseer, K. R.; Perumal, S.; Karthik, N.; Lee, Y. R., Highly Fluorescent Nitrogen-Doped Carbon Dots Derived from Phyllanthus Acidus Utilized as a Fluorescent Probe for Label-Free Selective Detection of $Fe^{3+}$ Ions, Live Cell Imaging and Fluorescent Ink. *Biosens. Bioelectron.* **2018,** *99*, 303-311.

S35. Durairaj, A.; Maruthapandi, M.; Luong, J. H. T.; Perelshtein, I.; Gedanken, A., Enhanced Uv Protection, Heavy Metal Detection, and Antibacterial Properties of Biomass-Derived Carbon Dots Coated on Protective Fabrics. *ACS Appl. Bio Mater.* **2022,** *5* (12), 5790-5799.

S36. Man, Y.; Li, Z.; Kong, W.-L.; Li, W.; Dong, W.; Wang, Y.; Xie, F.; Zhao, D.; Qu, Q.; Zou, W.-S., Starch Fermentation Wastewater as a Precursor to Prepare S,N-Doped Carbon Dots for Selective Fe(Iii) Detection and Carbon Microspheres for Solution Decolorization. *Microchem. J.* **2020,** *159*, 105338.

S37. Xu, J.; Wang, Y.; Sun, L.; Qi, Q.; Zhao, X., Chitosan and Kappa-Carrageenan-Derived Nitrogen and Sulfur Co-Doped Carbon Dots "on-Off-on" Fluorescent Probe for Sequential Detection of Fe(3+) and Ascorbic Acid. *Int. J. Biol. Macromol.* **2021,** *191*, 1221-1227.

S38. Nima, A. M.; Amritha, P.; Vidhya, L.; Subodh, G., Green Synthesis of Blue-Fluorescent Carbon Nanospheres from the Pith of Tapioca (Manihot Esculenta) Stem for Fe(Iii) Detection. *J. Mater. Sci. Mater. Electron.* **2020,** *31* (23), 21767-21778.

S39. Sawalha, S.; Silvestri, A.; Criado, A.; Bettini, S.; Prato, M.; Valli, L., Tailoring the Sensing Abilities of Carbon Nanodots Obtained from Olive Solid Wastes. *Carbon* **2020,** *167*, 696-708.

S40. Zhang, J.; Xia, A.; Chen, H.; Nizami, A. S.; Huang, Y.; Zhu, X.; Zhu, X.; Liao, Q., Biobased Carbon Dots Production Via Hydrothermal Conversion of Microalgae Chlorella Pyrenoidosa. *Sci. Total Environ.* **2022,** *839*, 156144.

S41. Zhu, L.; Li, D.; Lu, H.; Zhang, S.; Gao, H., Lignin-Based Fluorescence-Switchable Graphene Quantum Dots for Fe(3+) and Ascorbic Acid Detection. *Int. J. Biol. Macromol.* **2022,** *194*, 254-263.

S42. Zhang, Y.; Chan, K. F.; Wang, B.; Chiu, P. W. Y.; Zhang, L., Spore-Derived Color-Tunable Multi-Doped Carbon Nanodots as Sensitive Nanosensors and Intracellular Imaging Agents. *Sens. Actuators B Chem.* **2018,** *271*, 128-136.

S43. Zhao, S.; Song, X.; Chai, X.; Zhao, P.; He, H.; Liu, Z., Green Production of Fluorescent Carbon Quantum Dots Based on Pine Wood and Its Application in the Detection of $Fe^{3+}$. *J. Clean. Prod.* **2020,** *263*, 121561.

S44. Zulfajri, M.; Gedda, G.; Chang, C.-J.; Chang, Y.-P.; Huang, G. G., Cranberry Beans Derived Carbon Dots as a Potential Fluorescence Sensor for Selective Detection of $Fe^{3+}$ Ions in Aqueous Solution. *ACS Omega* **2019,** *4* (13), 15382-15392.

S45. Wang, R.; Jiao, L.; Zhou, X.; Guo, Z.; Bian, H.; Dai, H., Highly Fluorescent Graphene Quantum Dots from Biorefinery Waste for Tri-Channel Sensitive Detection of Fe(3+) Ions. *J. Hazard Mater.* **2021,** *412*, 125096.

S46. Jeong, G.; Park, C. H.; Yi, D.; Yang, H., Green Synthesis of Carbon Dots from Spent Coffee Grounds Via Ball-Milling: Application in Fluorescent Chemosensors. *J. Clean. Prod.* **2023,** *392*, 136250.